



HAL
open science

Anticancer effects of ikarugamycin and astemizole identified in a screen for stimulators of cellular immune responses

Shuai Zhang, Liwei Zhao, Mengfei Guo, Peng Liu, Sijing Li, Wei Xie, Ai-Ling Tian, Jonathan G Pol, Hui Chen, Hui Pan, et al.

► **To cite this version:**

Shuai Zhang, Liwei Zhao, Mengfei Guo, Peng Liu, Sijing Li, et al.. Anticancer effects of ikarugamycin and astemizole identified in a screen for stimulators of cellular immune responses. *Journal for Immunotherapy of Cancer*, 2023, 11 (7), pp.e006785. 10.1136/jitc-2023-006785 . hal-04159094

HAL Id: hal-04159094






<https://hal.science/hal-04159094v1>

Submitted on 11 Jul 2023

HAL is a multi-disciplinary open access archive for the deposit and dissemination of scientific research documents, whether they are published or not. The documents may come from teaching and research institutions in France or abroad, or from public or private research centers.

L'archive ouverte pluridisciplinaire **HAL**, est destinée au dépôt et à la diffusion de documents scientifiques de niveau recherche, publiés ou non, émanant des établissements d'enseignement et de recherche français ou étrangers, des laboratoires publics ou privés.

Anticancer effects of ikarugamycin and astemizole identified in a screen for stimulators of cellular immune responses

Shuai Zhang,^{1,2,3,4} Liwei Zhao,^{1,2} Mengfei Guo,³ Peng Liu,^{1,2} Sijing Li,^{1,2,4} Wei Xie ,^{5,6} Ai-Ling Tian,^{1,2} Jonathan G Pol ,^{1,2} Hui Chen ,^{1,2,4} Hui Pan,^{1,2,4} Misha Mao,^{1,2,4,7} Yumei Li,³ Laurence Zitvogel,^{8,9} Yang Jin ,³ Oliver Kepp ,^{1,2} Guido Kroemer^{1,2,10}

To cite: Zhang S, Zhao L, Guo M, *et al.* Anticancer effects of ikarugamycin and astemizole identified in a screen for stimulators of cellular immune responses. *Journal for ImmunoTherapy of Cancer* 2023;11:e006785. doi:10.1136/jitc-2023-006785

► Additional supplemental material is published online only. To view, please visit the journal online (<http://dx.doi.org/10.1136/jitc-2023-006785>).

SZ, LZ, MG and PL contributed equally.

Accepted 21 June 2023



© Author(s) (or their employer(s)) 2023. Re-use permitted under CC BY-NC. No commercial re-use. See rights and permissions. Published by BMJ.

For numbered affiliations see end of article.

Correspondence to

Dr Oliver Kepp;
captain.olsen@gmail.com

Guido Kroemer;
kroemer@orange.fr

Professor Yang Jin;
whuhjy@126.com

ABSTRACT

Background Most immunotherapies approved for clinical use rely on the use of recombinant proteins and cell-based approaches, rendering their manufacturing expensive and logistics onerous. The identification of novel small molecule immunotherapeutic agents might overcome such limitations.

Method For immunopharmacological screening campaigns, we built an artificial miniature immune system in which dendritic cells (DCs) derived from immature precursors present MHC (major histocompatibility complex) class I-restricted antigen to a T-cell hybridoma that then secretes interleukin-2 (IL-2).

Results The screening of three drug libraries relevant to known signaling pathways, FDA (Food and Drug Administration)-approved drugs and neuroendocrine factors yielded two major hits, astemizole and ikarugamycin. Mechanistically, ikarugamycin turned out to act on DCs to inhibit hexokinase 2, hence stimulating their antigen presenting potential. In contrast, astemizole acts as a histamine H1 receptor (H1R1) antagonist to activate T cells in a non-specific, DC-independent fashion. Astemizole induced the production of IL-2 and interferon- γ (IFN- γ) by CD4⁺ and CD8⁺ T cells both in vitro and in vivo. Both ikarugamycin and astemizole improved the anticancer activity of the immunogenic chemotherapeutic agent oxaliplatin in a T cell-dependent fashion. Of note, astemizole enhanced the CD8⁺/Foxp3⁺ ratio in the tumor immune infiltrate as well as IFN- γ production by local CD8⁺ T lymphocytes. In patients with cancer, high H1R1 expression correlated with low infiltration by TH1 cells, as well as with signs of T-cell exhaustion. The combination of astemizole and oxaliplatin was able to cure the majority of mice bearing orthotopic non-small cell lung cancers (NSCLC), then inducing a state of protective long-term immune memory. The NSCLC-eradicating effect of astemizole plus oxaliplatin was lost on depletion of either CD4⁺ or CD8⁺ T cells, as well as on neutralization of IFN- γ .

Conclusions These findings underscore the potential utility of this screening system for the identification of immunostimulatory drugs with anticancer effects.

WHAT IS ALREADY KNOWN ON THIS TOPIC

⇒ Most immunotherapies approved for clinical use rely on the use of recombinant proteins and cell-based approaches, rendering their manufacturing expensive and logistics onerous. The identification of novel small molecule immunotherapeutic agents might overcome such limitations.

WHAT THIS STUDY ADDS

⇒ Here we employed a dendritic cell (DC) screening platform to identify ikarugamycin and astemizole as novel immunopharmacological agents that activate DCs and T cells, respectively. Both ikarugamycin and astemizole improved the anticancer activity of the immunogenic chemotherapeutic agent oxaliplatin in a T cell-dependent fashion.

HOW THIS STUDY MIGHT AFFECT RESEARCH, PRACTICE OR POLICY

⇒ The combination of astemizole with the standard of care chemotherapeutic oxaliplatin was able to eradicate orthotopic non-small cell lung cancers while inducing a state of protective long-term immune memory in a murine model. This underscores the utility of this screening system for the mode of action-agnostic identification of immunostimulatory drugs.

INTRODUCTION

Since 2005 it has become clear that traditional anticancer treatment modalities including chemotherapy and radiotherapy are particularly efficient if they succeed in inducing anticancer immune responses.^{1–4} This led to the a posteriori realization that successful anticancer therapies that initially had been conceived for their cancer cell-autonomous cytotoxic effects were indeed ‘accidental’ immunotherapies.^{5,6} Over the past decade a series of immuno-oncology drugs have been clinically approved. Such immunotherapies

comprise a vast array of distinct agents ranging from immune checkpoint inhibitors (mostly targeting cytotoxic T-lymphocyte associated protein 4 (CTLA-4), programmed cell death 1 (PD-1), programmed death-ligand 1 (PD-L1)) to cytokines, immunogenic cell death (ICD) inducers, oncolytic viruses, dendritic cell (DC) vaccines, as well as chimeric antigen receptors (CAR) T cells.^{7–13} With the sole exception of ICD inducers, which can be small molecules (as recently exemplified by lurbinectedin, an inhibitor of DNA-to-RNA transcription approved for the treatment of relapsed small-cell lung cancer),¹⁴ FDA/EMA (Food and Drug Administration/European Medicines Agency-approved immunotherapies are usually either recombinant proteins or even cell-based, rendering their manufacturing expensive and logistics onerous. For this reason, it may be useful to identify new immunotherapeutic agents among small molecule libraries.¹⁵

Recently, we have developed a sort of miniature cellular immune system involving two cell types that both are immortalized and hence can be amplified without limits.^{16,17} The first cell type is a conditionally immortalized DC precursor from C57Bl/6 mice that can be continuously cultured in the presence of the glucocorticoid dexamethasone (DEX) and the tetracycline (TET) doxycycline (DOX, which activates the TET-on promoter of SV40 large T-cell antigen to inactivate the tumor suppressors RB and TP53). These cells can be differentiated into immature DCs in vitro on removal of DEX and DOX to generate de-induced/de-immortalized DCs (de-iniDCs).¹⁸ Such de-iniDCs are capable of engulfing protein antigens and then presenting their antigenic peptides bound to major histocompatibility complex (MHC) class I molecules (eg, K^b from C57BL/6 mice) to cytotoxic T lymphocytes (CTL).^{16–18} The second immortalized cell type is the B3Z hybridoma generated by the fusion of T lymphocytes recognizing the K^b-restricted chicken ovalbumin (OVA)-derived peptide (SIINFEKL corresponding to residues 257–264 of OVA) with a leukemia cell line.¹⁹ In this system, de-iniDCs pulsed with OVA protein present the OVA-derived SIINFEKL peptide to B3Z cells, which then respond by producing interleukin-2 (IL-2). We have used this ‘miniature immune system’ to characterize genetic defects affecting DC function (as exemplified by the knockout of *Fpr1*) and to identify Toll-like receptor 3 ligands as potential immunostimulators.^{16,17}

Here, we report the results of three medium-throughput screening campaigns performed on co-cultures of de-iniDCs and B3Z cells. We unravel the identification of one compound that acts on DCs to improve antigen presentation, as well as that of another agent that rather acts as a non-specific activator of T-cell function. We show that both agents are endowed with the potential to improve anticancer immunosurveillance in preclinical experiments, supporting the contention that this kind of mechanism-agnostic immunopharmacological screen can lead to the identification of novel anticancer agents, as well as to their mechanistic deconvolution.

RESULTS

Identification of astemizole and ikarugamycin as immunostimulatory agents

For the identification of drugs capable of activating the DC-CTL dialog, we took advantage of de-iniDCs that were cultured for 16 hours in the presence of different drugs, then washed twice and pulsed with OVA protein for 4 hours, washed again twice, and then co-cultured with B3Z hybridoma cells (which are specific for the OVA-derived peptide SIINFEKL presented by MHC class I K^b protein) for 16 hours. Then, the supernatant of cells was harvested to measure the production of IL-2 following established protocols¹⁷ (figure 1A). This screen was performed on three different libraries, namely the ICCB library of known bioactive compounds (figure 1B, all tested at 1 μM), the Prestwick library mostly comprising approved drugs (figure 1C, all tested at 1 μM) and a homemade neurotransmitter library (online supplemental table S1, figure 1D, all tested at 5 μM). In the ICCB library (480 compounds), the strongest hit was ikarugamycin, an antibiotic that has been described to activate the pro-autophagic transcription factor transcription factor EB (TFEB)²⁰ and to inhibit the enzymatic activity of hexokinase 2.²¹ Astemizole, which is a histamine receptor antagonist,²² as well as an inhibitor of KCNH1 and KCNH2 potassium channels,²³ was identified as a common hit in the two other screens involving the Prestwick library (1200 compounds) and the neurotransmitter library (659 small molecules) (figure 1C,D). Both ikarugamycin and astemizole caused a dose-dependent increase in the capacity of OVA-pulsed de-iniDCs and bone marrow-derived dendritic cells (BMDCs) to stimulate IL-2 production by B3Z cells (figure 1E,F, online supplemental figure S1). No other drugs could be confirmed to be active in independent validation experiments. As a result, we focused the subsequent mode of action studies on ikarugamycin and astemizole.

Validation of ikarugamycin as a DC stimulator

BMDCs cultured in the presence of ikarugamycin (but not astemizole) exhibited an upregulation of activation markers including CD40, CD80, CD86 and MHC class II (MHC-II). This ikarugamycin effect was higher than the one observed with the positive control, bacterial liposaccharide (LPS) (figure 1A, online supplemental figure S1B,C). Highly purified ikarugamycin from distinct suppliers was similarly potent (online supplemental figure S1A). Ikarugamycin exhibited no cytotoxic effects on BMDCs or de-iniDCs (online supplemental figure S1D), and its effects were not inhibited (and rather enhanced) by polymyxin B, which did suppress LPS effects on de-iniDCs and BMDCs, in accord with its known inhibitory effects on endotoxin-mediated signaling (online supplemental figure S1E-N). Beta-2 microglobulin is encoded by the *B2m* gene and is required for MHC class I complex formation. Using *B2m* knockout de-iniDCs, we confirmed that MHC class I expression by de-iniDCs is required for the stimulation of antigen presentation by ikarugamycin

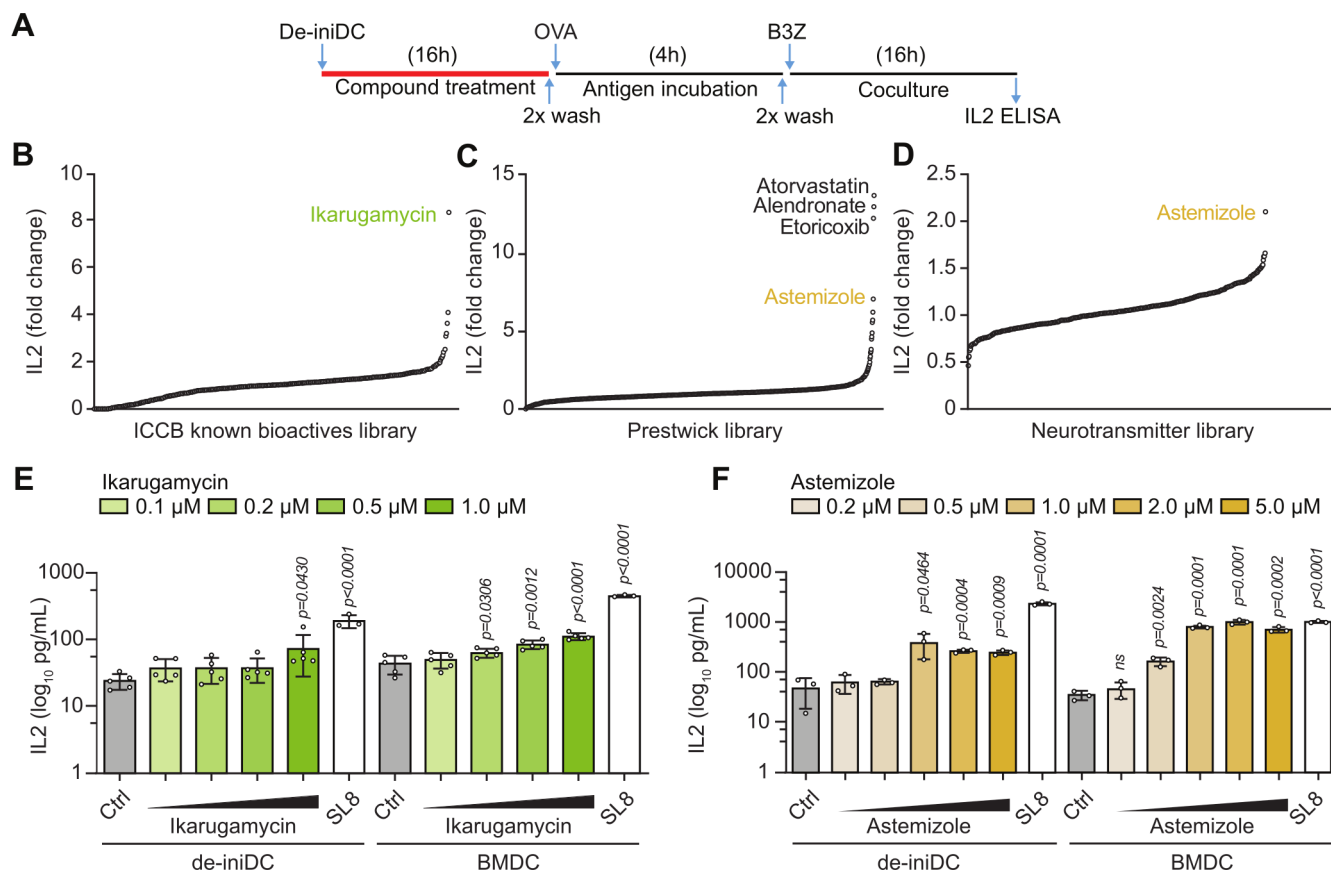


Figure 1 Identification of astemizole and ikarugamycin as immunostimulatory agents. (A–D) De-ini dendritic cells (DC) were cultured with the compounds of the indicated chemical libraries for 16 hours, then washed twice and pulsed with 500 $\mu\text{g}/\text{mL}$ ovalbumin (OVA) protein for 4 hours, washed again twice, and then co-cultured with B3Z hybridoma cells for 16 hours. Then, the supernatant of cells was harvested and the production of interleukin 2 (IL2), as an indicator for antigen cross-presentation capacity, was measured by ELISA. IL2 concentration was normalized according to dimethyl sulfoxide (DMSO)-treated controls. (E–F) De-iniDCs and bone marrow-derived DCs (BMDCs) were treated with DMSO or ikarugamycin (0.1, 0.2, 0.5, 1 μM) (E), or astemizole (0.2, 0.5, 1, 2, 5 μM) (F) for 16 hours, then washed twice and pulsed with OVA protein or 10 ng/mL OVA257-264 peptide (SL8, as a positive control) for 4 hours, washed again twice, and then co-cultured with B3Z hybridoma cells. IL-2 secretion was measured by ELISA as an indication for antigen cross-presentation capacity. Data are reported as the mean \pm SD of three replicates, and statistical analyses were performed with a two-tailed unpaired Student's t test. de-iniDCs, de-induced/de-immortalized DCs.

(online supplemental figure S1O,P). Of note, BMDCs cultured in the presence of ikarugamycin exhibited a dose-dependent reduction of hexokinase 2 (figure 2B,C), which has previously been shown to inhibit DC function.²⁴ Accordingly, small interfering RNA (siRNA)-induced knockdown of hexokinase 2 in BMDCs (figure 2D,E) phenocopied the effects of ikarugamycin in thus far that it increased the capacity of OVA-pulsed BMDCs to stimulate IL-2 production by B3Z cells (figure 2F) and enhanced the expression levels of CD40, CD80, CD86 and MHC-II on BMDC (figure 2G). When injected into established cutaneous MCA205 fibrosarcomas implanted in immunocompetent C57BL/6 mice, ikarugamycin failed to reduce tumor growth. However, ikarugamycin enhanced the efficacy of systemic chemotherapy with the ICD inducer oxaliplatin, hence reducing tumor growth and increasing mouse survival (figure 2H–J, online supplemental figure S2A,B). In addition, the combination treatment with ikarugamycin+oxaliplatin was particularly efficient in

increasing the frequency of mature DCs (phenotype: F4/80⁺CD11c⁺CD86⁺) in the tumor (online supplemental figure S2C,D). Of note, the antitumor efficacy of this combination (ikarugamycin+oxaliplatin) was entirely lost on depletion of T lymphocytes by injecting antibodies capable of depleting CD4⁺ and CD8⁺ cells (figure 2L–M, online supplemental figure S2E,F).

In conclusion, it appears that ikarugamycin stimulates DC function by inhibiting hexokinase 2. Moreover, ikarugamycin can be used to stimulate anticancer immune responses elicited by oxaliplatin.

Validation of astemizole as a T-cell stimulator

Since astemizole failed to directly activate DCs (figure 2A), we wondered whether it might act on T lymphocytes rather than on antigen presenting cells. For this, we either added astemizole to DC (de-iniDCs or BMDCs) during pulsing with OVA and eliminated it from the cultures by four washes (figure 3A, protocol α) instead of the two washes

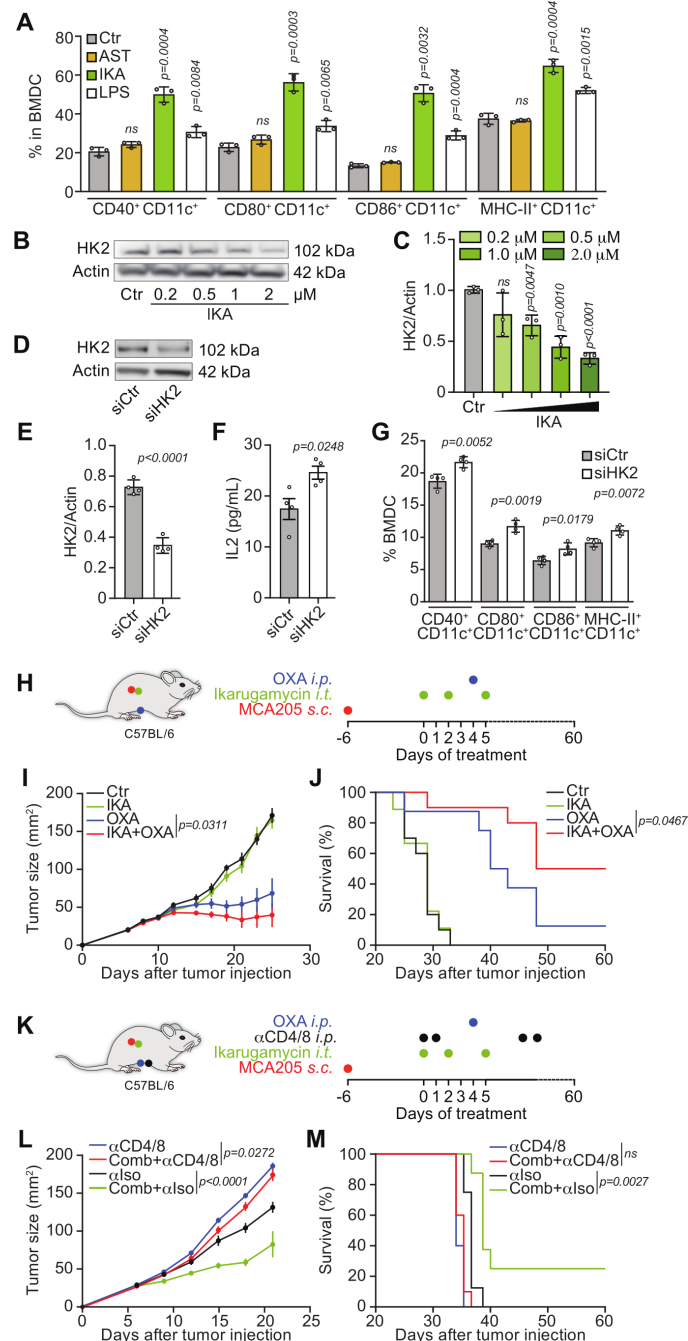


Figure 2 Validation of ikarugamycin as a dendritic cell (DC) stimulator. (A) Bone marrow-derived dendritic cells (BMDCs) were treated with ikarugamycin (IKA; 1 μ M) or astemizole (AST; 1 μ M) for 16 hours then DC activation and maturation was analyzed by flow cytometry, 1 μ g/mL of lipopolysaccharide (LPS) was used as positive control. (B, C) BMDCs were treated with IKA (0.2, 0.5, 1, 2 μ M) for 16 hours, then cells were harvested, and proteins were detected by western blot. (D–E) Representative western blot images (D) and quantification (E) of control (Ctr) or hexokinase 2 (Hk2) knockdown BMDC cells. (F) Ctr or Hk2 knockdown BMDCs were pulsed with 500 μ g/mL ovalbumin (OVA) protein for 4 hours, washed twice, and then co-cultured with B3Z hybridoma cells for 16 hours. Interleukin 2 (IL2) secretion was measured by ELISA as an indicator for antigen cross-presentation capacity. (G) Control (Ctr) or Hk2 knockdown BMDCs were collected for cytofluorometric detection of DC activation and maturation markers. (H) Schematic overview of the treatment of murine MCA205 fibrosarcoma with IKA (0.2 mg/kg) and oxaliplatin (OXA; 10 mg/kg), alone or in combination. (I, J) The tumor growth curves (I, mean \pm SEM) and Kaplan-Meier overall survival (J) of murine fibrosarcoma MCA205 cells in C57BL/6 mice (n=8–10 mice /group). (K) Schematic overview of the treatment of murine MCA205 fibrosarcoma with IKA plus OXA (Comb) and neutralizing antibodies to CD4 and CD8 (α CD4/CD8), alone or in combination. (L, M) The tumor growth curves (L, mean \pm SEM) and Kaplan-Meier overall survival (M) of murine fibrosarcoma MCA205 cells in immunocompetent and antibody-neutralized C57BL/6 mice (n=8–10 mice/group). Data are reported as the mean \pm SD of three replicates, and statistical analyses were performed with two-tailed unpaired Student's t test (A, C, E, F, G), and two-way analysis of variance followed by the Holm-Šidák post hoc test (I, L). Log-rank test was used for survival comparison.

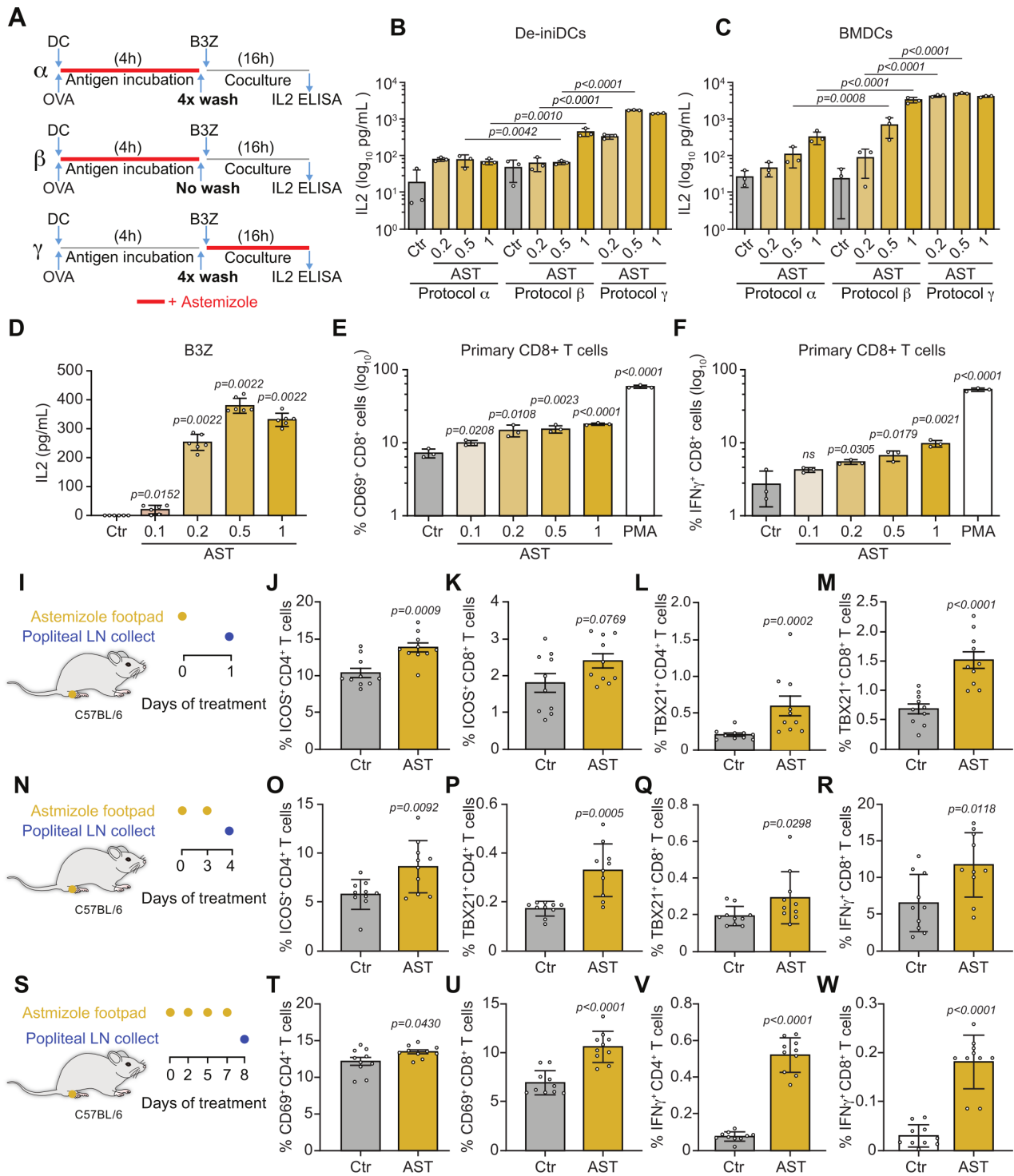


Figure 3 Validation of astemizole as a T-cell stimulator. (A) Schematic overview of different protocols for astemizole treatment. (B, C) De-ini dendritic cells (DC)s (B) and bone marrow-derived DCs (C) were treated with dimethyl sulfoxide (DMSO) or astemizole (AST; 0.2, 0.5, 1 μ M) in different protocol, and then co-cultured with B3Z hybridoma cells. Interleukin 2 (IL2) secretion was measured by ELISA as an indicator for antigen cross-presentation capacity. (D) B3Z hybridoma cells were treated with DMSO or AST (0.1, 0.2, 0.5, 1 μ M) for 16 hours. IL2 secretion was measured by ELISA as an indicator for antigen cross-presentation capacity. (E, F) Mouse primary CD8⁺ T cells were treated with DMSO, or AST (0.1, 0.2, 0.5, 1 μ M) or phorbol myristate acetate (PMA; 50 ng/mL) for 16 hours, followed by 5-hour treatment with brefeldin A (5 μ g/mL), and analyzed for expression of the indicated proteins or cytokines using flow cytometry. (I–W) AST was injected at 1 mg/kg body weight into the hind footpad either once (I), twice (N) or four times (S). The draining (popliteal) lymph nodes were collected and dissociated into single cell suspensions. Then the cells were treated with brefeldin A (5 μ g/mL) for 5 hours, and analyzed for expression of the indicated proteins or cytokines using flow cytometry (n=5 mice /group). Each dot represents one lymph node. Data are reported as the mean \pm SD, and statistical analyses were performed with two-tailed unpaired Student's t test (B, C, E, F, J, K, M, O, R, T, U), and Mann-Whitney U test (D, L, P, Q, V, W). de-iniDCs, de-induced/de-immortalized DCs.

used in the screen (figure 1A) before adding B3Z cells. Alternatively, no washes were performed at all (figure 3A, protocol β) or astemizole was added late, after four washes, together with B3Z cells (figure 3A, protocol γ). Quantitative comparison of the dose responses obtained by these three protocols by measuring IL-2 production by B3Z cells suggested that astemizole was most efficient when it acted on B3Z cells (figure 3B,C). Indeed, the addition of astemizole to B3Z cells cultured alone (in the absence of DCs) was sufficient to stimulate IL-2 production. When added to primary T lymphocytes isolated from the spleen, astemizole caused a dose-dependent increase in the expression of the activation marker CD69 (figure 3E, online supplemental figure S3A), the production of interferon- γ (IFN- γ) (figure 3F). Astemizole also increased the proliferation of primary CD8⁺ T lymphocytes isolated from mouse spleens (online supplemental figure S3B). In a subsequent series of experiments, we injected astemizole into the hind footpad from adult C57Bl/6 mice either once (figure 3I–M, online supplemental figure S3C), twice (figure 3N–R) or four times (online supplemental figure S3S–W) and determined the phenotype of the T cells present in the draining (popliteal) lymph node. This procedure revealed the capacity of astemizole to induce the acquisition of activation markers (such as CD69 and inducible T cell costimulator (ICOS)), the expression of the transcription factor TBX21 (which is required for the generation of TH1 and TC1 cells, ie, T cells exhibiting the capacity to produce IFN- γ),²⁵ as well as the production of IFN- γ by both CD4⁺ and CD8⁺ T cells (figure 3I–W).

In conclusion, it appears that astemizole is able to stimulate a TH1/TC1 profile of T-cell activation leading to the generation of IL-2 and IFN- γ by CD4⁺ and CD8⁺ T cells.

Non-specific T-cell stimulation by astemizole

In a next series of experiments, we determined the capacity of astemizole to stimulate human T cells. When added to Jurkat T cells, astemizole caused the rapid (3 min) activation of the T-cell receptor-proximal signaling kinases, as detectable by immunoblot detection of activating phosphorylations affecting LAT (on tyrosine residue 220) LCK (on tyrosine 394) and ZAP-70 (on tyrosine 319) (figure 4A–D). Using a biosensor cell line (Jurkat-LCK) that allows to measure LCK activation in real-time (see Materials and methods), we found that astemizole caused LCK activation within 6 min of addition (figure 4E, online supplemental figure S4A). Addition of a pharmacological LCK inhibitor (6-(2,6-dimethylphenyl)-2-((4-(4-methylpiperazin-1-yl)phenyl)amino)benzo[4,5]imidazo[1,2-a]pyrimido[5,4-e]pyrimidin-5(6H)-one) did not only abolish the astemizole-induced activation of the LCK biosensor (figure 4E) and the phosphorylation of LCK (figure 4F) but also inhibited the astemizole-elicited expression of IFN- γ and CD69, as determined by immunofluorescence and cytometry, as well as the secretion of ELISA-detectable IL-2 and

IFN- γ by B3Z cells (figure 4G–J, online supplemental figure S4B) as well as by primary CD8⁺ T lymphocytes (figure 4K–M). As to be expected for a T-cell activator,²⁶ astemizole also induced rapid Ca²⁺ fluxes in T cells, as determined by means of the fluorescent Ca²⁺ biosensor Indo-1 (online supplemental figure S4C). Chelation of intracellular Ca²⁺ by means of 1,2-Bis(2-aminophenoxy) ethane-N,N,N',N'-tetraacetic acid tetrakis(acetoxymethyl ester) (BAPTA-AM) abolished the production of IL-2 and IFN- γ (online supplemental figure S4D,E).

Altogether, these results indicate that astemizole has the capacity to stimulate human and mouse T cells in a non-specific fashion.

Antihistaminergic mode of action of astemizole

Astemizole has been introduced into the clinics as a histamine receptor H1 antagonist,²² yet has been withdrawn from the market because of its arrhythmogenic side effects mediated by inhibition of KCNH1 and KCNH2 potassium channels.²³ Of note, the capacity of astemizole to enhance IFN- γ and IL-2 production by B3Z and primary CD8⁺ T cells was inhibited in a dose-dependent fashion when millimolar concentrations of histamine or micromolar concentrations of histamine trifluoromethyl toluidide (HTMT, a mixed H1/H2 histamine receptor agonist) or micromolar concentrations of 2-pyridylethylamine dihydrochloride (a H1 histamine receptor agonist) were simultaneously added (figure 55A–F, online supplemental figure S5A,B). Histamine and HTMT also inhibited the astemizole-driven activating phosphorylation of LCK (figure 5G). However, the capacity of astemizole to enhance IL-2 production by B3Z was not blocked by the specific H2 histamine receptor agonists amthamine dihydrobromide (amthamine) and dimaprit dihydrochloride (dimaprit), nor by the H3 histamine receptor agonist imetit dihydrobromide (imetit) and the H4 histamine receptor agonist 4-methylhistamine (online supplemental figure S5C–F). Moreover, several selective H1 antagonists including desloratadine, ketotifen, promethazine and terfenadine²⁷ shared the capacity of astemizole to activate LCK (figure 5H). To finally validate the inhibitory role of histamine receptor H1 (HRH1) on T-cell activation, we took advantage of *Hrh1* knockout mice (online supplemental figure S5G). Primary T cells isolated from such mice exhibited a constitutively increased expression of IFN- γ that could not be further enhanced by astemizole (figure 5I). Furthermore, as compared with wild type controls, freshly isolated splenic CD4⁺ and CD8⁺ T cells from *Hrh1*^{-/-} mice exhibited an increased spontaneous production of IFN- γ , and *Hrh1*^{-/-} spleens harbored less FOXP3⁺CD4⁺ regulatory T cells (Tregs) (figure 5J–L, online supplemental figure S5H).

Altogether, these results indicate that astemizole acts as an HRH1 antagonist to stimulate T-cell activation.

Anticancer immunity-stimulating effects of astemizole

As described above for ikarugamycin, astemizole on its own had no anticancer effects. Thus, repeated

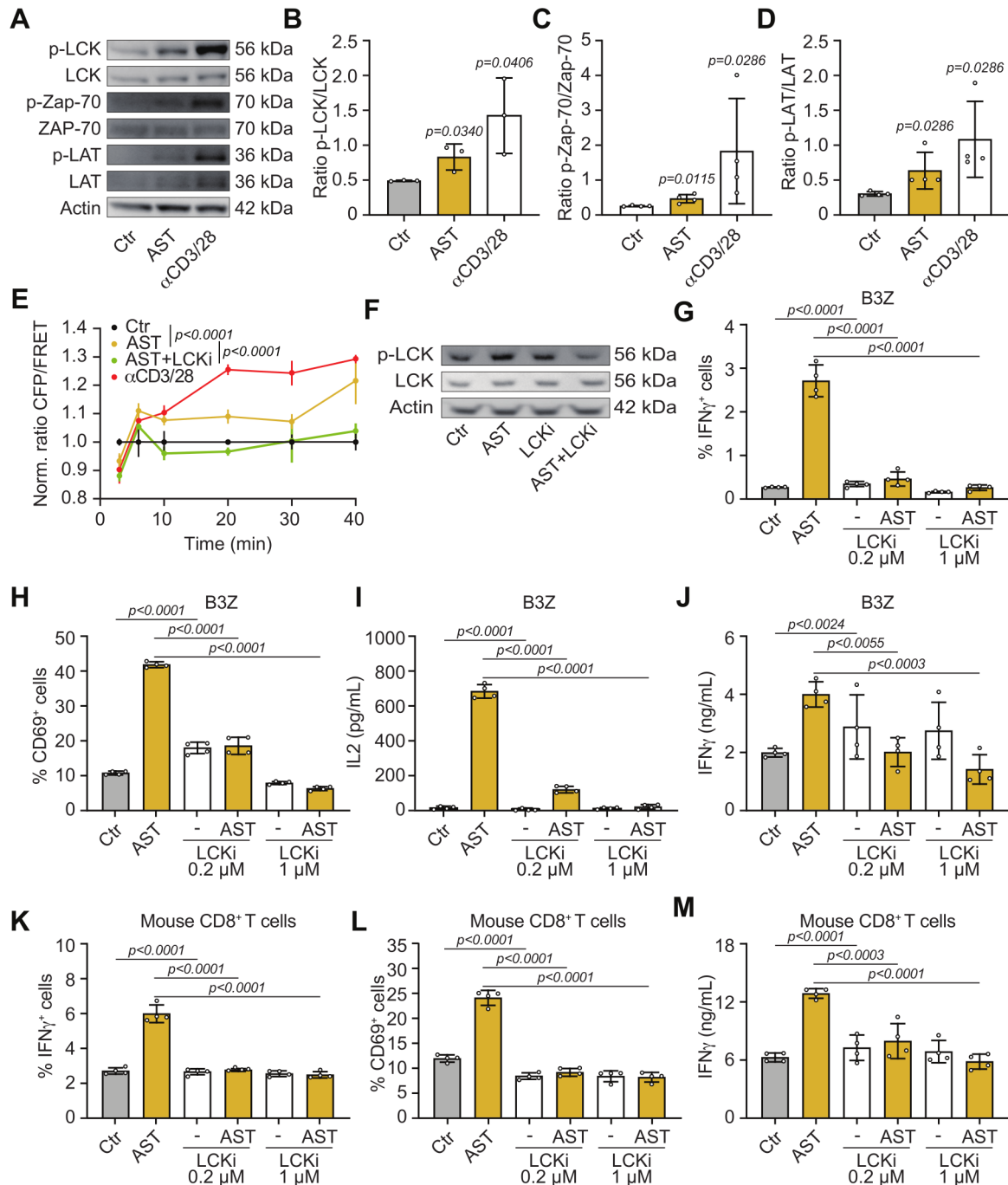


Figure 4 Non-specific T-cell stimulation by astemizole. (A–D) Jurkat T cells were treated with astemizole (AST; 1 μM) and human CD3/CD28 dynabeads (10^6 cells per 25 μL) for 3 min and were then analyzed by western blotting. Representative western blot images (A) and quantification of p-LCK (tyr 394) to LCK (B), p-Zap-70 (tyr 319) to Zap-70 (C), and p-LAT (tyr 220) to LAT (D). (E) Jurkat-LCK T cells were treated with dimethyl sulfoxide (DMSO), AST (1 μM), AST (1 μM) plus LCK inhibitor (LCKi; 1 μM), and human T Cell TransAct nanobeads (10^5 cells per μL) in different time points and were measured by flow cytometry. (F) Jurkat T cells were pre-treated with DMSO or LCKi (1 μM) for 30 min, and treated with DMSO or AST (1 μM) for 3 min, then cells were harvested, and proteins were detected by western blot. (G–J) B3Z hybridoma cells were treated with AST (1 μM) alone or in combination with LCKi (0.2, 1 μM) for 16 hours, the cell supernatant was collected for the quantification of interleukin 2 (IL-2) and interferon gamma (IFN- γ) secretion by ELISA (I, J). While the remaining cells were treated with brefeldin A (5 μg/mL) for 5 hours, and analyzed for expression of CD69 or IFN- γ using flow cytometry (G, H). (K–M) Mouse primary CD8⁺ T cells were treated with AST (1 μM) alone or in combination with LCKi (0.2, 1 μM) for 16 hours, the cell supernatant was collected for the quantification of IFN- γ secretion by ELISA (M). While the remaining cells were treated with brefeldin A (5 μg/mL) for 5 hours, and analyzed for expression of CD69 or IFN- γ using flow cytometry (K, L). Data are reported as the mean \pm SD, statistical analyses were performed with two-tailed unpaired Student's t test (B), Mann-Whitney U test (C, D), one-way analysis of variance (ANOVA) followed by the Holm-Šidák post hoc test (G–M), and two-way ANOVA followed by the Holm-Šidák post hoc test (E).

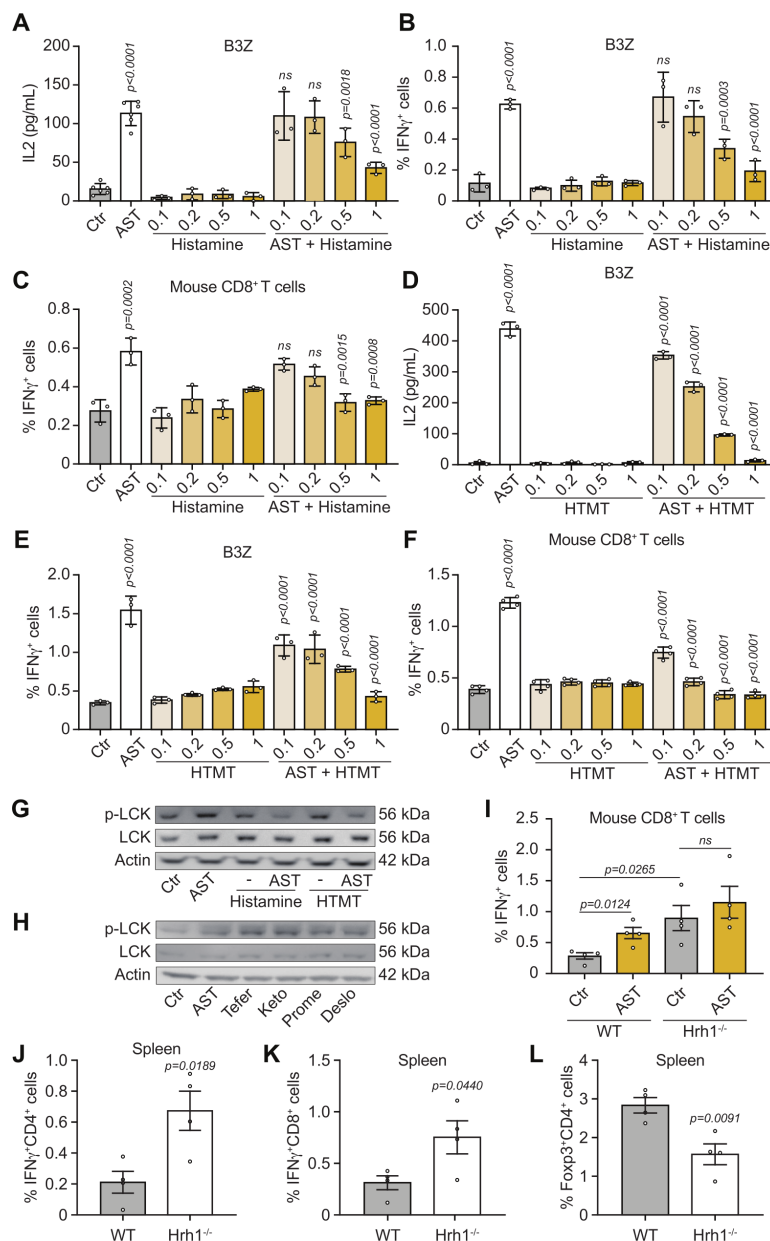


Figure 5 Antihistaminergic mode of action of astemizole. (A, B) B3Z hybridoma cells were treated with astemizole (AST; 1 μ M) alone or in combination with histamine (0.5, 1, 2, 5 mM) for 16 hours, the cell supernatants were collected for the quantification of interleukin 2 (IL2) secretion by ELISA (A). While the remaining cells were treated with brefeldin A (5 μ g/mL) for 5 hours, and analyzed for expression of interferon gamma (IFN- γ) using flow cytometry (B). (C) Mouse primary CD8 $^+$ T cells were treated with AST (1 μ M) alone or in combination with histamine (0.5, 1, 2, 5 mM) for 16 hours, followed by 5 hours of brefeldin A (5 μ g/mL), and analyzed for expression of IFN- γ using flow cytometry. (D, E) B3Z hybridoma cells were treated with astemizole (1 μ M) alone or in combination with HTMT dimaleate (0.5, 1, 2, 5 μ M) for 16 hours, the cell supernatants were collected for the quantification of IL2 secretion by ELISA (D). While the remaining cells were treated with brefeldin A (5 μ g/mL) for 5 hours, and analyzed for expression of IFN- γ using flow cytometry (E). (F) Mouse primary CD8 $^+$ T cells were treated with AST (1 μ M) alone or in combination with HTMT dimaleate (0.5, 1, 2, 5 μ M) for 16 hours, followed by 5 hours of brefeldin A (5 μ g/mL), and analyzed for expression of IFN- γ using flow cytometry. (G) Jurkat T cells were pretreated with DMSO, histamine (5 mM) or HTMT dimaleate (5 μ M) for 30 min, and treated with DMSO or AST (1 μ M) for 3 min, then cells were harvested, and proteins were detected by western blot. (H) Jurkat T cells treated with AST, tefernadine (Tefer), ketotifen fumarate (Keto), promethazine (Prome) and desloratadine (Deslo) all at 1 μ M for 3 min were analyzed by western blotting. (I) Mouse primary CD8 $^+$ T cells isolated from wild type or *Hrh1* $^{-/-}$ knock out C57BL/6 mice were treated with DMSO or AST (1 μ M) for 16 hours, followed by 5 hours of brefeldin A (5 μ g/mL), and analyzed for expression of IFN- γ using flow cytometry (n=4 mice /group, Data are reported as the mean \pm SEM). (J–L) Spleens from wild-type C57BL/6 or *Hrh1* $^{-/-}$ mice were harvested dissociated into single cell suspensions, then the cells were treated with brefeldin A (5 μ g/mL) for 5 hours, and analyzed for expression of the indicated proteins or cytokines using flow cytometry (n=4 mice /group, Data are reported as the mean \pm SEM). Data are reported as the mean \pm SD, and statistical analyses were performed with two-tailed unpaired Student's t test (I–L), and one-way analysis of variance followed by the Holm-Šidák post hoc test (A–F).

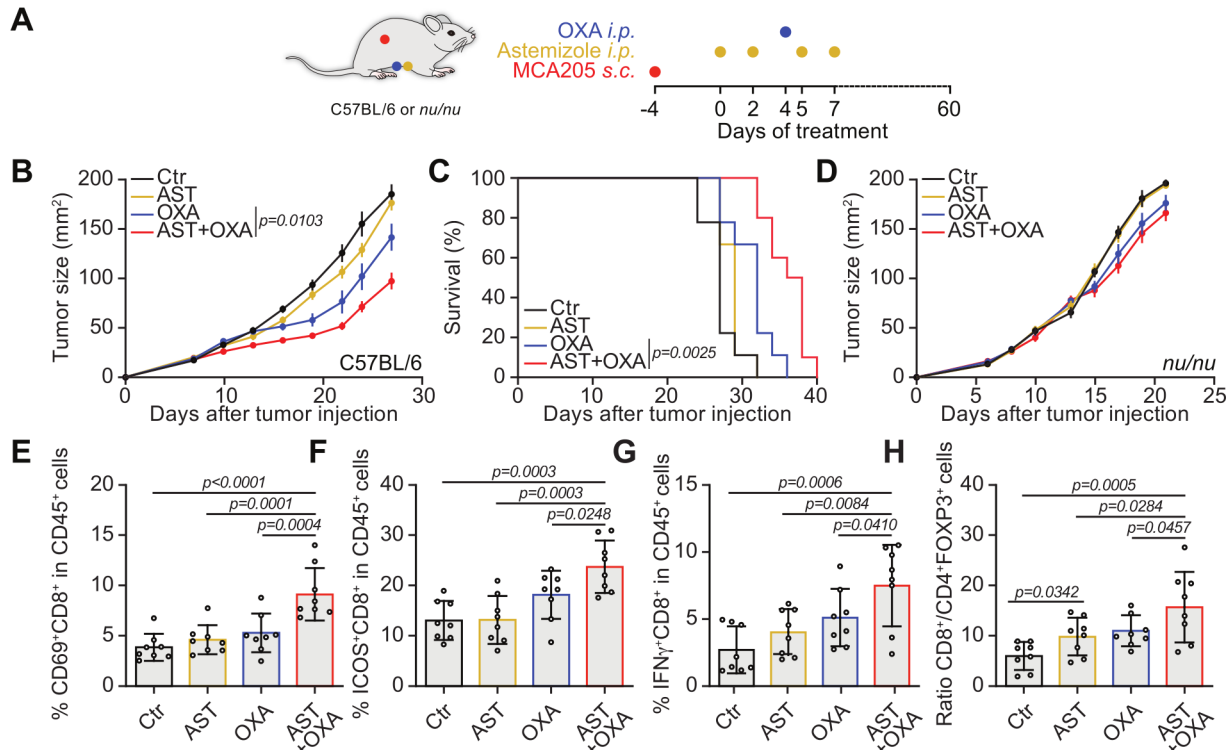


Figure 6 Astemizole enhances antitumor effect of immunogenic chemotherapy. (A) Schematic overview of the treatment of murine MCA205 fibrosarcoma with astemizole (AST) and oxaliplatin (OXA), alone or in combination (Comb). (B, C) The tumor growth curves (B, mean±SEM) and Kaplan-Meier overall survival (C) of murine fibrosarcoma MCA205 cells in C57BL/6 mice (n=9–10 mice /group). (D) The tumor growth curves (mean±SEM) of murine fibrosarcoma MCA205 cells in *nu/nu* mice (n=10 mice /group). (E–H) MCA205 fibrosarcoma bearing mice were treated as in (A) and were euthanized on day 15 after tumor injection, tumors were harvested and dissociated into single cell suspensions, and analyzed for expression of the indicated proteins or cytokines using flow cytometry. Data are reported as the mean±SD, and statistical analyses were performed with one-way analysis of variance followed by the Holm-Šidák post hoc test (E–H), and two-way analysis of variance followed by the Holm-Šidák post hoc test (B, D). Log-rank test was used for survival comparison (C).

intraperitoneal (*i.p.*) injections of astemizole failed to reduce the growth of orthotopic MCA205 fibrosarcomas *in vivo*. However, astemizole enhanced the tumor growth-decelerating and animal survival-extending effect of oxaliplatin (figure 6A–C, online supplemental figure S6A,B). No such effect was found in *nu/nu* mice lacking mature T cells due to athymia (figure 6D). Indeed, in tumors implanted in normal, immunocompetent mice, the combination of astemizole and oxaliplatin induced signs of CD8⁺ T-cell activation (CD69 and ICOS expression), IFN- γ production as well as an improvement of the ratio of CD8⁺ CTL over CD4⁺Foxp3⁺ Tregs (figure 6E–H, online supplemental figure S6C). In addition, the combination treatment with astemizole+oxaliplatin was particularly efficient in improving the CTL/Treg ratio and increasing the frequency of bona fide DCs (phenotype: F4/80⁺CD11c⁺MHC-II⁺) in the tumor draining lymph node (online supplemental figure S6D-F).

In a further series of experiments, we tested the effects of astemizole against TC-1 non-small cell lung cancers and E0771 breast cancers implanted under the skin. Again, astemizole used as a standalone agent failed to exhibit major anticancer effects but exhibited activity in combination with other agents. Ectopic, subcutaneous explanted TC-1 tumors only reduced their growth in

response to a triple combination of astemizole, oxaliplatin and PD-1 blockade, not to any of the single agents or dual combinations (online supplemental figure S6G-L). Moreover, astemizole enhanced the capacity of oxaliplatin to reduce the growth of ectopic subcutaneous E0771 breast cancer and the survival of tumor-bearing mice (online supplemental figure S6M-Q). In an orthotopic model in which intravenously injected luciferase-expressing TC-1 cells developed cancers within the lung, astemizole alone did exhibit significant anticancer effect. Moreover, astemizole improved the anticancer effect of oxaliplatin. This was visible both at the level of intrathoracic TC1 tumor growth monitored by bioluminescence imaging, as well as at the level of mouse survival (figure 7A–D, online supplemental figure S7A,B). Rechallenge of two mice cured with astemizole alone, five mice cured with oxaliplatin alone and nine mice cured with the combination (astemizole plus oxaliplatin) with subcutaneously injected TC1 cells revealed the establishment of a state of permanent immunity against these cancer cells, which could not form tumors any more on rechallenge. This immunity was specific because antigenically distinct MCA205 fibrosarcomas readily grew on most mice (figure 7E–F, online supplemental figure S7C,D). Of note, the depletion of either CD4⁺ or CD8⁺ T cells,

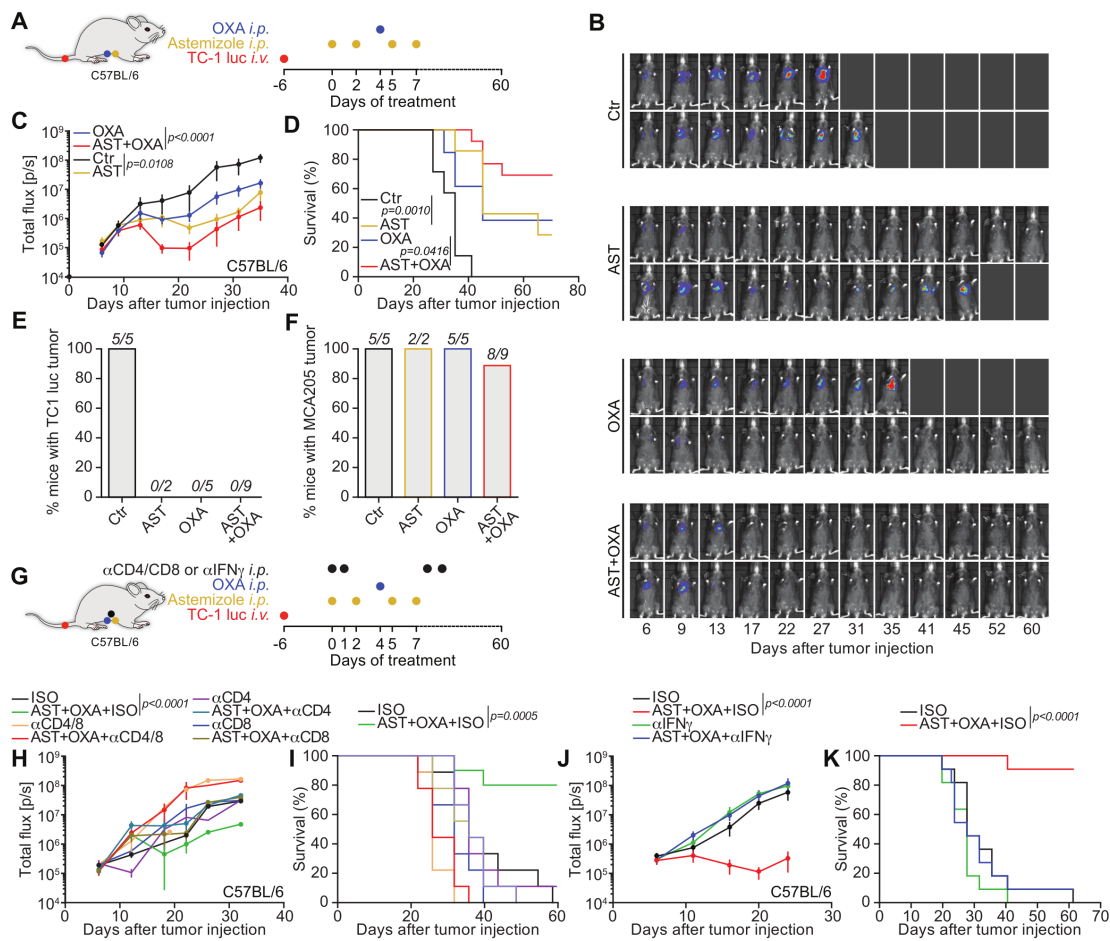


Figure 7 Astemizole induces immune-dependent anticancer efficacy in orthotopic TC-1-luc lung cancer model. (A) Schematic overview of the treatment of murine orthotopic TC-1-luc lung cancer with astemizole (AST) and oxaliplatin (OXA), alone or in combination (Comb). (B–D) Representative bioluminescence images of tumor development under different treatment conditions are shown in (B), the quantification of bioluminescence signals was used to indicate tumor size and is reported as tumor growth curves (C, mean±SEM) and Kaplan-Meier overall survival (D) of murine orthotopic TC-1-luc lung cancer cells in C57BL/6 mice (n=7–13 mice/group). (E, F) Cured immunocompetent mice were rechallenged with living cancer cells of the same type (TC-1-luc), as well as of a different type (MCA205), the percentage of TC-1-luc tumor growth on cured mice is shown in (E) and the percentage of MCA205 tumor growth on cured mice is shown in (F). (G) Schematic overview of the treatment of murine orthotopic TC-1-luc lung cancer with AST plus OXA (Comb) in combination with neutralizing antibodies to CD4 and/or CD8 or IFN- γ , or the isotype (ISO) control antibodies (n=9–11 mice /group). (H–K) The quantification of bioluminescence signals was used to indicate tumor size and reported as tumor growth curves (H, J, mean±SEM) and Kaplan-Meier overall survival (I, K) of murine orthotopic TC-1-luc lung cancer in immunocompetent and antibody-neutralized C57BL/6 mice. Statistical analyses were performed with two-way analysis of variance followed by the Holm-Šidák post hoc test (C), (H, J). Log-rank test was used for survival comparison (D, I, K).

as well as the antibody-mediated neutralization of IFN- γ , fully abolished the anticancer effects of the combination (astemizole plus oxaliplatin) against orthotopic TC-1 lung cancers, underscoring the decisive contribution of both T lymphocyte populations to the therapeutic effect (figure 7G–K, online supplemental figure S7E–L).

In conclusion, it appears that non-specific T-cell activation by astemizole can improve the anticancer effects of immunogenic chemotherapy in an IFN- γ -dependent fashion.

Immunosuppressive effects of HRH1 on the immune infiltrate in patients with cancer

The aforementioned results suggest that astemizole acts as an HRH1 antagonist to improve cancer immunosurveillance, prompting us to investigate the potential impact of HRH1 on the cancer immune infiltrate. A pan-cancer analysis performed on The Cancer Genome Atlas (TCGA), revealed positive correlations between HRH1 messenger RNA (mRNA) and several myeloid cell subsets but negative correlations with between HRH1 mRNA and multiple distinct T lymphocyte subset. This anticorrelation was most pronounced for the CD4⁺ TH1 subset (online supplemental figure S8A), in line with the strong capacity of astemizole to stimulate the production of the

TH1 cytokines IL-2 and IFN- γ observed in preclinical experiments (figures 1 and 4–6). Moreover, HRH1 mRNA levels positive correlated with multiple genes associated to Tex-related T-cell exhaustion (online supplemental figure S8B), as well as an elevated ratio of exhausted over effector, naïve and memory CD8⁺ T cells (online supplemental figure S8C) across multiple different cancer types.

In essence, these results suggest that HRH1 negatively impacts on cancer immunosurveillance.

DISCUSSION

Here, we unveil the results of a demonstration project dealing with the identification of immunostimulatory small molecules that favor IL-2 production by T cells that respond to DCs presenting a model antigen. Three independent screens employing this system led to the identification and subsequent validation and mechanistic characterization of two drugs, astemizole and ikarugamycin, which both turned out to stimulate the immune control of cancers in preclinical models, though through rather distinct mechanisms.

Ikarugamycin was found to stimulate the antigen presenting function of DCs, presumably through an inhibitory effect on hexokinase 2, which normally restrains DC function.²⁴ It should be noted that hexokinase 2 is also a target for clotrimazole, a drug that can be administered systemically (by *i.p.* injection) into tumor-bearing immunocompetent mice to reduce tumor growth as a monotherapy.²⁴ In sharp contrast, ikarugamycin had no anticancer effects if injected systemically (not shown) and had to be administered intratumorally to increase the therapeutic efficacy of oxaliplatin-based chemotherapy. Hence, ikarugamycin is clearly inferior to clotrimazole in its anticancer activity. Notwithstanding this limitation, the identification of such a hexokinase-2-targeting drug underscores the utility of the screening procedure that we developed.

From the preclinical and clinical points of view, the identification of astemizole as an immunostimulatory agent appears much more interesting. It should be noted that astemizole was identified in the present paper—to some degree—by serendipity, likely because the two washes performed in the screen (to remove free OVA and free drug from the supernatant of drug/OVA-treated de-iniDCs) allowed for carryover of astemizole to B3Z cells. Indeed, a more careful procedure (with four washes), as well as a whole series of experiments on DC alone or on DC-free B3Z cells (or primary T cells as well as human Jurkat acute T lymphocytic leukemia cells) revealed that astemizole acted on T cells (not DCs) to cause their non-specific activation, as indicated by the activating phosphorylation of several kinases (LAT, LCK and ZAP-70) within minutes, the induction of Ca²⁺ fluxes, activation markers (CD69, ICOS), enhanced expression of TBX21, as well as the production of the TH1 cytokines IFN- γ and IL-2. Such effects were obtained *in vitro* (on B3Z cells, primary mouse T cells, as well as human Jurkat cells) and

in vivo, both in tumor-free mice receiving injections of astemizole into the footpad (on T lymphocytes located in the draining popliteal node) and in tumor-bearing mice under oxaliplatin-based chemotherapy (on the intratumoral immune infiltrate and the tumor-draining inguinal lymph node). More importantly, astemizole was able to amplify the tumor growth-reducing effect of oxaliplatin in three different models of malignant disease (cutaneous fibrosarcomas, breast cancer or non-small cell lung cancer (NSCLC)), and these effects were lost on depletion of either CD4⁺ or CD8⁺ T cells or on neutralization of IFN- γ , demonstrating that they are indeed secondary to an effect on T lymphocytes.

It should be noted that the immunostimulatory effects of astemizole on T cells are mediated by an inhibitory effect on HRH1, based on the facts that other HRH1 receptor antagonists have similar T cell activating effects, that a molar excess of histamine or a more selective H1 agonist (HTMT) abolish the astemizole effect, and that the knockout of HRH1 in mice phenocopies the astemizole effect. Importantly, in mouse models, HRH1 antagonists are known to stimulate the anticancer effects of immune checkpoint blockade by means of antibodies specific CTLA-4 or PD-1.²⁸ However, this effect has been attributed to the prevention of the histamine-induced polarization of macrophages to an M2-like immunosuppressive phenotype with upregulation of the immune checkpoint V-domain Ig suppressor of T cell activation (VISTA).²⁸ The immunostimulatory effect of astemizole may be clinically relevant because the use of specific antihistamines (including astemizole) is linked to overall survival of patients with localized ovarian cancer²⁹ and any type of non-localized cancers,³⁰ as well as to favorable outcome of immunotherapy in a pan-cancer analysis.³¹ Moreover, clinical responses to PD-1 blockade negatively correlate with circulating histamine levels.²⁸ Hence, the immunostimulatory effects of HRH1 antagonists are likely to be patient-relevant. In favor of this conjecture, we found that in patient-derived tumors high expression of HRH1 mRNA apparently has a negative impact on the composition of the cancer immune infiltrate, correlating with a relative underabundance of CD4⁺ Th1 cells, an upregulation of Tex-related exhaustion markers, as well as a higher ratio of exhausted over effector, naïve and memory CD8⁺ T cells. Such findings were obtained for many cancers across the oncological spectrum suggesting a broad immunosuppressive effect for HRH1.

Irrespective of mechanistic details that may require further investigation, it appears that the screening procedure that we applied to several publicly available drug libraries has the potential to identify therapeutically and clinically relevant drugs. Encouraged by these findings, we are now in the starting block to perform even larger drug screens on proprietary compound collections.

MATERIALS AND METHODS

Cell culture and related reagents

RPMI-1640 medium (Cat# 61870010), DMEM medium (Cat# 10566016), HEPES (CAT# 15630056), sodium pyruvate (Cat# 11360070), phosphate-buffered saline (PBS, Cat# 20012027), penicillin-streptomycin (Pen/Strep, 10000 U/mL, Cat# 15140122), and TrypLE Express (Cat# 12604013) were purchased from Life Technologies (Carlsbad, California, USA). Fetal bovine serum (FBS, Cat# F7524), β -mercaptoethanol (Cat# M3148), dexamethasone (Cat# D0700000), and doxycycline hyclate (Cat# D3000000) were purchased from Sigma (St. Louis, Missouri, USA). Recombinant murine GM-CSF (Cat# 315-03), recombinant murine IL-2 (Cat# 212-02), recombinant murine IL-4 (Cat# 214-14), recombinant murine IL-7 (Cat# 217-17) were obtained from PeproTech (Cranbury, New Jersey, USA). Unless otherwise indicated, all plasticware was purchased from Corning Life Sciences (Corning, New York, USA). RPMI-1640 with 10% de complemented FBS, 1 mM sodium pyruvate, 10 mM HEPES, and 1 \times Pen/Strep was used as a basic DC/T cell medium.

The B3Z hybridoma T cells were kindly provided by Sebastian Amigorena and maintained with DC/T cell medium supplemented with β -mercaptoethanol (50 μ M). Jurkat cells were maintained with DC/T cell medium supplemented with β -mercaptoethanol (50 μ M). Jurkat cells stably expressing ZapLck biosensors (Jurkat-LCK) were established by electroporation with ZapLck biosensor (addgene, plasmid #131584) were maintained with DC/T cell medium supplemented with β -mercaptoethanol (50 μ M) and puromycin (1 μ g/mL).³² The inducible-immortalized dendritic cell line (iniDCs) were kindly shared by Cornelia Richter and colleagues,¹⁸ and maintained with DC/T cell medium supplemented with β -mercaptoethanol (50 μ M) and recombinant mouse GM-CSF (at a final concentration of 10 ng/mL). IniDCs are immortalized under the induction of Dex/Dox (Dexamethasone at 100 nM+Doxycycline at 2 μ M). iniDCs were de-induced (in the absence of Dex/Dox) for 4 days to immature DCs ('de-iniDCs') and were used for further experiments. MCA205 fibrosarcoma, E0771 breast cancer cells, TC-1 NSCLC cells and TC-1 cells expressing firefly luciferase (TC-1-luc) were cultured with DMEM medium containing 10% de complemented FBS and 1 \times Pen/Strep.

Chemicals and antibodies

The neurotransmitter library compounds were purchased from Enzo Life Sciences (Lörrach, Germany), the ICCB known bioactives library compounds were purchased from Biomol GmbH (Hamburg, Germany), The Prestwick chemical library was obtained from Prestwick Chemical (Illkirch, France). Lipopolysaccharides (LPS, Cat# L2654), Ionomycin from *Streptomyces conglobatus* (Cat# I9657), Phorbol 12-myristate 13-acetate (PMA, Cat# P8139), histamine (Cat# Y0001779), oxaliplatin (Cat# PHR1528), albumin from chicken egg white (OVA, Cat# A5503) were obtained from Sigma-Aldrich (St. Louis, Missouri, USA). OVA 257-264 peptide (SL8,

Cat# vac-sin) was obtained from Invivogen (San Diego, California, USA). Ikarugamycin was obtained from Enzo Life Sciences (Cat# BML-EI313-0500, Farmingdale, New York, USA), MedChemExpress (Cat. No.: HY-119764, 500 μ g, Monmouth Junction, New Jersey, USA) and Cayman (Item No. 15386, Ann Arbor, Michigan, USA). Polymyxin B sulfate salt (Cat# P4932-5MU), Dexamethasone (Cat# D0700000), and Doxycycline hyclate (Cat# D3000000) were purchased from Sigma (St. Louis, Missouri, USA). Amthamine dihydrobromide (Cat# NH-100), dimaprit dihydrochloride (Cat# NH-102) and imetit dihydrobromide (Cat# AC-284) were obtained from Enzo Life Sciences. Astemizole (sc-201088), 2-Pyridylethylamine dihydrochloride (sc-203467) and 4-methylhistamine dihydrochloride (sc-203475A) were purchased from Santa Cruz Biotechnology (Dallas, Texas, USA). 1,2-Bis(2-aminophenoxy)ethane-N,N,N',N'-tetraacetic acid tetrakis(acetoxymethyl ester, BAPTA-AM, Cat# B1205) and Indo-1-AM (I1203), Dynabeads human T-activator CD3/CD28 for T Cell expansion and activation (Cat# 11131D) were purchased from Thermo Fisher Scientific (Waltham, Massachusetts, USA). LCK inhibitor (6-(2,6-dimethylphenyl)-2-((4-(4-methylpiperazin-1-yl)phenyl)amino)benzo[4,5]imidazo[1,2-a]pyrimido[5,4-e]pyrimidin-5(6H)-one, Cat# HY-12072) was purchased from MedChemExpress. Luciferin potassium salt was purchased from Promega (Madison, Wisconsin, USA).

ON-TARGETplus non-targeting control siRNAs (D-001810-01-05) and On-TARGETplus mouse HK2 (L-051128-00-0005) siRNA were obtained from Horizon Discovery (Cambridge, UK). ZapLck biosensor (Plasmid #131584) was obtained from Addgene (Watertown, Massachusetts, USA).³²

P3 primary cell 4D-Nucleofector X Kit S (Cat# V4XP-3032) was purchased from Lonza (Basel, Switzerland). Tumor dissociation kit (Cat# 130-096-730) and T cell TransAct (Cat# 130-111-160) were purchased from Miltenyi Biotec.

Antibodies for western blot: α Hexokinase II (Cat# 2867) α Phospho-Zap-70 (Tyr319)/Syk (Tyr352) (Cat# 2701), α Zap-70 (Cat# 2705), α Phospho-LAT (Tyr220) (Cat# 3584), and α LAT (Cat#45533) were purchased from Cell Signaling Technology (Danvers, Massachusetts, USA). α Phospho-LCK (Tyr394) (Cat#933102), α LCK (Cat# 601002) were from BioLegend (San Diego, California, USA). Antibodies for ELISA, including ELISA MAX deluxe set mouse IL-2 (Cat#431004) and ELISA MAX deluxe set mouse IFN- γ (Cat#430816) were from BioLegend. In vivo neutralizing antibodies to PD-1 (Cat# BE0273), CD4 (Cat# BE0003-1), CD8 (Cat# BE0061), IFN- γ (Cat# BE0055), and corresponding isotype controls (Cat# BE0088, Cat# BE0090) were purchased from Bio X Cell (Lebanon, New Hampshire, USA). Mouse monoclonal antibodies employed for flow cytometry: α β 2-microglobulin PE (Cat# 154504), α FOXP3 FITC (Cat# 11-5773-82), LIVE/DEAD Fixable Yellow (Cat# L34959), α CD8a FITC (Cat# 11-0081-82), α IL-2 PE-cy7 (Cat# 25-7029-42), α IFN- γ APC (Cat#17-7319-82), α F4/80

PE-Cyanine7 (Cat# 25-4801-82) were purchased from eBioscience. α CD8a APC/Fire 750 (Cat# 100766), α CD8a PE (Cat# 100708), α CD45 Alexa Fluor 647 (Cat# 103124), α CD45 APC-Cyanine7 (Cat# 103116), α CD16/32 (Cat# 101302), α CD11c APC (Cat# 117310), α ICOS Pacific Blue (Cat# 313522), α CD69 PE (Cat# 104508), α I-A/I-E BV605 (Cat# 107639), α I-A/I-E PerCP/Cyanine5.5 (Cat# 107626), α CD4 PE (Cat# 100408), α CD40 PE (Cat# 124610), α CD80 Alexa Fluor 488 (Cat# 104716), α CD86 BV650 (Cat# 105036), α CD86 APC-Fire750 (Cat# 105046) were purchased from BioLegend. α CD3 BUV737 (Cat# 612803), α CD4 BUV496 (Cat# 612952), α T-bet BV786 (Cat# 564141), α CD4 BV421 (Cat# 562891), α CD11c BUV395 (Cat# 744180) were obtained from BD Biosciences (Franklin Lakes, New Jersey, USA).

Knockout of *B2m* in iniDCs

CRISPR mediated gene knockouts in iniDCs were performed as previously published.¹⁷ CRISPR Reagents including Edit-R Lentiviral CAG-Blast-Cas9 Nuclease Particles (Cat#: VCAS10129), Edit-R CRISPR-Cas9 Synthetic tracrRNA (Cat#: U-002005–50), DharmaFECT 1 Transfection Reagent (Cat#: T-2001–04), and pre-designed crRNA targeting *B2m* (Cat# CM-062465-01-0002, target sequence: AGTATACTCACGCCACCCAC) were all purchased from Dharmacon, Horizon Discovery (Waterbeach, UK). To knockout *B2m*, the iniDCs were seeded in 6-well plates at 1×10^5 cells/well in 2 mL DC/T medium and let adapt for 6 hours before adding 3 μ L of LentiGuide Cas9 lentiviral particles (MOI of 0.3 TU/cell) and gentle shaking. The cells were incubated for 48 hours and then the supernatant was replaced with 2 mL fresh DC/T medium for the transfection of synthetic guide RNA. The synthetic guide RNA complex was prepared by adding equal quantities of crRNA targeting *B2m*+tracrRNA, all at a final concentration of 25 nM, in 100 μ L serum-free RPMI-1640 medium and incubation for 5 min at room temperature. Transfection reagent was prepared by diluting 10 μ L of DharmaFECT 1 in 100 μ L of RPMI-1640 medium and incubation for 5 min at room temperature. The crRNA:tracrRNA complex and DharmaFECT 1 working solutions were then mixed and incubated for another 20 min before addition to lentiviral-transduced iniDCs, which were then incubated for another 48 hours for efficient gene knockout. Transfected cells were then single cell sorted into 96-well plates using a BD FACSAria cell sorter. About 2 weeks later, clones were picked and duplicated for biobanking and flow cytometry detection of *B2m* expression, either with or without stimulation by recombinant IFN- γ employed at a final concentration of 1000 IU/mL.

Animals and cancer models

Female wild-type C57BL/6 mice, 6–8 weeks old, and female athymic nude (*nu/nu*) mice were purchased from ENVIGO France (Gannat, France), and were maintained in a specific pathogen-free (SPF) environment with a 12 hours light-dark cycle at 21–23°C and

40–60% humidity in the preclinical evaluation platform at the Gustave Roussy Cancer Campus, France. Female HRH1^{-/-} mice were purchased from Cyagen Biosciences (Suzhou) (Suzhou, China) and were maintained in a SPF environment with a 12-hour light-dark cycle at 21–23°C and 40–60% humidity in the animal center of the Tongji Medical College, HuaZhong University of Science and Technology, China. All animal experiments were approved by the Animal Care Committee of Gustave Roussy Campus Cancer Center (2022_053_39463).

One hundred μ L of MCA205, E0771, or TC-1 cell suspension containing 5×10^5 cells were inoculated subcutaneously into the right lower flank of C57BL/6 or athymic nude (*nu/nu*) mice. When tumors became palpable, mice were randomized and received the treatments described below. Tumor surface was then regularly monitored and tumor lesions that exceeded 200 mm² were euthanized. The tumor volume was calculated using the formula: surface=length \times width \times $\pi/4$. Orthotopic NSCLC models were established as previously published.³³ For TC-1 orthotopic tumor model, 100 μ L of TC-1-luc cell suspension containing 5×10^5 cells were intravenously injected to C57BL/6 mice. Tumor incidence and development were monitored by using bioluminescence imaging, when tumor incidence in the lung was detected at an exposure time of 4 min on day 6 after tumor injection, mice were randomized and received the treatments described below.

Immunoblotting

All reagents used for immunoblotting were purchased from Life Technologies. Protein extraction was conducted in radioimmunoprecipitation assay buffer containing phosphatase and protease inhibitors (Life Technologies, Cat# A32961), 1 \times SDS Loading Buffer, and 1 \times Sampling Reducing Buffer. After denatured at 100°C, proteins were separated on NuPAGE Bis-Tris gels in the NuPAGE MOPS SDS Running Buffer and electro-transferred to 0.45 μ m polyvinylidene fluoride membranes (Bio-Rad, Hercules, California, USA). After 1 hour block with 5% skim milk powder/tris-buffered saline (TBS)–0.1% tween (TBST), membranes were incubated with primary antibodies overnight at 4°C. Membranes were then washed three times with TBST and incubated with horseradish peroxidase (HRP)-conjugated secondary antibodies (Southern Biotechnologies, Birmingham, Alabama, USA) for 1 hour at room temperature. After three times washing with TBST, blots were subjected to chemiluminescence-based detection using the Amersham ECL Prime kit, on an ImageQuant LAS 4000 imager (GE Healthcare, Piscataway, New Jersey, USA). Beta-actin antibody was used to control equal loading.

Genotyping

Genotyping was performed by conventional PCR on genomic DNA isolated from mouse-tails using standard procedures according to the instruction of Quick Genotyping Assay Kit for Mouse Tail (Cat# D7283S, Beyotime, China). For genotyping of knockouts two pair of primers

were used: primer 1 for wild-type allele (forward primer 5'-TGACCACATAACCTTAAACTGTAGT-3'; reverse primer 5'-TGCCTAATTTCTAGCAACTCTGA-3') and primer 2 for *hrh1* knockout allele (forward primer 5'-TCATAGCTTGGCATCTTTGTCAC-3'; reverse primer 5'-TGTGACCAGGAGATACTACTTAG-3'), which resulted in a product of 794bp for the wild-type allele and 611 bp for the knockout allele.

Bioluminescence imaging

Bioluminescence images were acquired on an IVIS Lumina III imaging system (Caliper Life Sciences, Hopkinton, Massachusetts, USA) as previously described.³³ Eight minutes before mouse tumor bioluminescence imaging, 150 mg/kg body weight of beetle luciferin potassium salt dissolved in DPBS (Promega, Madison, Wisconsin, USA) were injected intraperitoneally into mice. Two minutes before imaging, mice were anesthetized with vaporized isoflurane. Tumor bearing with total flux more than 10^8 were euthanized.

Chemical and antibody treatment in vivo

The solvent (Sol) used for ikarugamycin is PBS, and for astemizole is corn oil. For footpad injection, mice were anesthetized with vaporized isoflurane, 1 mg/kg body weight astemizole or corn oil were injected into the footpad, following the schedule specified in the figures and corresponding legends. For cancer treatment, ikarugamycin was administrated intratumorally at a dose of 0.2 mg/kg body weight while astemizole was administrated *i.p.* at a dose of 10 mg/kg body weight, and following the schedule specified in the figures and corresponding legends. At 8 days after tumor injection, oxaliplatin (10 mg/kg body weight) or 5% glucose solution were injected *i.p.* into each mouse. In case of combination with checkpoint blockade, mice received *i.p.* injection of 200 µg anti-PD-1 (clone 29F.1A12, Bio X Cell) antibody or equal amounts of isotype control antibody (clone LTF-2, Bio X Cell) at 8, 12 and 16 days after oxaliplatin treatments. For T-cell depletion, mice received *i.p.* injection of 100 µg anti-CD8 (clone 2.43 Bio X Cell), anti-CD4 (clone GK1.5 Bio X Cell), or their combination, or equal amounts of isotype control antibody (clone LTF-2, Bio X Cell) at 6, 7, 12, and 18 days after tumor injection. For IFN- γ neutralization, mice received 300 µg anti-IFN- γ (clone XMG1.2, Bio X Cell) or equal amounts of isotype control antibody (clone HRPN, Bio X Cell) at 6, 7, 12, and 18 days after tumor injection.

Generation of BMDCs

BMDCs were prepared from bone marrow precursors as described by Son *et al.*³⁴ Bone marrow cells were collected from the *tibia* and *femur* of 8–10 weeks old C57BL/6 mice, after red blood cell lysis, bone marrow cells were seeded at a density of 5×10^6 cells per 15 × 15 mm petri dish and cultured at 37°C in DC/T cell medium supplemented with β -mercaptoethanol (50 µM), 20 ng/mL recombinant mouse GM-CSF and 10 ng/mL recombinant mouse IL-4.

On days 3 and 6, half of the medium was replaced with fresh medium and BMDCs were used on day 7.

Isolation of CD8⁺ T cells in vitro

Mouse CD8⁺ T cells were prepared as previously described.³⁵ Splens and lymph nodes from wild-type C57BL/6 or HRH1^{-/-} mice were harvested and filtered through a 70 µm cell strainer to generate a single-cell suspension. CD8⁺T cells were isolated by using mouse CD8 naïve T-cell isolation kit (BioLegend) and then plated in DC/T cell medium supplemented with β -mercaptoethanol (50 µM), 20 ng/mL recombinant mouse IL-2 (PeproTech) and 10 ng/mL recombinant mouse IL-7 (PeproTech). For activated T cells, cells were cultured in 48-well plates coated with 5 µg/mL anti-CD3 (clone 145–2C11, BioLegend) and 2.5 µg/mL anti-CD28 (clone 37.51, BioLegend) antibodies for 48 hours and then transferred to uncoated plates for at least 24 hours before use.

Electroporation

The P3 primary cell 4D-Nucleofector X kit S (Lonza) was used for nucleofection. For BMDCs knockdown, cells were harvested on day 6. Five hundred thousand cells per reaction were resuspended in 20 µL of P3 primary nucleofection solution (Lonza). Twenty pmol of HK2 siRNA or non-targeting control siRNA were added to solution and then loaded into the supplied nucleofector cassette strip (Lonza). The strip was inserted into the Lonza 4D-Nucleofector and electroporated with the buffer P3, DN-100 condition. After electroporation, 80 µL prewarmed DC/T medium was immediately added into each well and placed at room temperature for 10 min. Then, cells were transferred into a 24 well plate and cultured in DC/T medium supplemented with β -mercaptoethanol (50 µM), 20 ng/mL recombinant mouse GM-CSF (PeproTech) and 10 ng/mL recombinant mouse IL-4 (PeproTech). Three days after nucleofection, the transfected BMDCs were used for further experiments. For the transfection of Jurkat cells, cells were passaged the day before electroporation. Two hundred thousand cells per reaction were resuspended in 20 µL of P3 primary nucleofection solution (Lonza). Then 1 µg zapLck biosensor plasmid DNA was added to 20 µL cell/P3 nucleofection solution and loaded into the supplied nucleofector cassette strip (Lonza). The strip was inserted into the Lonza 4D-Nucleofector and nucleofected with the Buffer P3, CL-120 condition. After nucleofection, 80 µL prewarmed DC/T medium was immediately added into each cassette well and placed at room temperature for 10 min. Then, cells were transferred into 24 well plate and cultured in DC/T medium supplemented with β -mercaptoethanol (50 µM). Two days after nucleofection, 1 µg/mL of puromycin was added into the medium for selection.

Intracellular calcium measurement

Intracellular calcium was determined using the Indo-1 AM according to the manufacturer's instructions. Fluorescence was measured using a BD FACSCanto II Flow

Cytometer with 355 nm excitation, 379/28 and 515/30 emission filter.

In vitro antigen cross-presentation assay

In vitro antigen cross-presentation assay was done as previously described.^{17,36} BMDCs or de-iniDCs (2.5×10^5 cells/mL) were seeded in 96-well plates (200 μ L/well) and treated with indicated compounds for 16 hours, after washed or not with PBS, soluble OVA was added into the cell culture at a final concentration of 500 μ g/mL and incubated for 4 hours at 37°C and 5% CO₂. Then the BMDCs or de-iniDCs were centrifuged at 400 \times g for 5 min and washed or not with PBS again. After removing the supernatant from DCs, 200 μ L/well of B3Z (2.5×10^5 cells/mL) suspension was added and co-incubated with DCs for 18 hours at 37°C and 5% CO₂.

ELISA analysis

Cell culture supernatants of B3Z, DC-B3Z or mouse CD8⁺ T cells were collected by spinning at 1000 \times g for 10 min at 4°C. The level of IL-2 and IFN- γ in the cell supernatants was quantified by means of an ELISA (ELISA MAX Deluxe Set Mouse IL-2 and ELISA MAX Deluxe Set Mouse IFN- γ) according to the manufacturer's instructions. The absorbance at 450 nm was measured using a BMG FLUOstar plate reader (BMG Labtech, Offenburg, Germany).

Tissue dissociation and flow cytometric analysis

Lymph nodes from mice were harvested and filtered through a 70 μ m cell strainer to generate a single-cell suspension. Seven days after chemotherapy, MCA205 fibrosarcoma tumors were harvested, weighed, and then processed before phenotyping immune cells as described before.³⁷ In brief, tumors were collected in gentleMACS C Tubes (Miltenyi Biotec; Bergisch Gladbach, Germany) containing 1 mL RPMI-1640 medium on ice. Then tumors were dissociated using the gentleMACS dissociator with a mouse tumor dissociation kit (Miltenyi Biotec) according to the manufacturer's instructions. For flow cytometry staining, PBS with 1% BSA were used as flow cytometry buffer. For cell surface staining, cells were incubated with LIVE/DEAD Yellow Fixable dye in cold PBS for 10 min to label dead cells followed by incubating with antibodies against CD16/CD32 in flow cytometry buffer for 10 min to block Fc receptors. For multiplex staining, cells were incubated with a panel of fluorescence-conjugated antibodies in cold flow cytometry buffer for 30 min surface staining in the dark. In case of intracellular staining, cells were incubated with brefeldin A (5 μ g/mL) in CTL-Test Medium (Cellular Technology Limited, Cleveland, Ohio, USA) containing 2 mM L-Glutamine for 5 hours before surface staining. For intracellular staining, the surface-labeled cells were permeabilized and fixed using a Foxp3/Transcription Factor Staining Buffer kit (eBioscience) according to the manufacturer's instructions. Then antibodies against FOXP3, IFN- γ , or T-bet were stained for another 30 min. Cells without intracellular staining were fixed with 4% PFA (Sigma). All the cells were kept

at 4°C before flow cytometric analysis. Cell acquisition was performed with a BD LSRFortessa X-20 flow cytometer (BD Biosciences) and data were analyzed using the FlowJo software (BD Biosciences). All the detailed gating strategies for the flow cytometric analysis are provided in online supplemental figures.

Bioinformatic analysis

The correlation of HRH1 expression and immune cell infiltration level was analyzed based on RNA sequencing (RNA-seq) data from the TCGA database (<https://portal.gdc.cancer.gov/>). RNA-seq data were converted to TPM (transcripts per million reads) format and log₂ converted. The immune infiltrate was estimated using the xCELL and TIMER2.0 data sets.^{38,39} Spearman's correlation coefficients were calculated for HRH1 expression (log₂ TPM) and distinct immune cell subsets on a linear scale. The association of HRH1 and Tex-related marker genes was analyzed based on log₂(TPM+1) format RNA-seq data from TCGA database. TCGA RNA-seq data were used to perform single gene differential analyses by stratifying patients with high (above median) or low expression (below median) of HRH1 for each cancer type. Immunologic signatures were explored with c7.all.v7.2.symbols.gmt gene set from MSigDB Collections database. Genes upregulated in exhausted vs naive CD8 T cells (GSE9650_NAIVE_VS_EXHAUSTED_CD8_TCELL_DN), and genes upregulated in exhausted versus memory CD8 T cells (GSE9650_EXHAUSTED_VS_MEMORY_CD8_TCELL_UP) were analyzed using Gene Set Enrichment Analysis analysis. The CD8 T cell-related exhaustion signatures were shown in bubble plots with information of normalized enrichment score, gene count, and p value.⁴⁰ The statistical analysis and visualization are performed with R (V.3.6.3) and R packages, including DESeq2 (V.1.26.0), clusterProfiler (V.3.14.3), and ggplot2 (V.3.3.3).^{41–43}

Statistical analysis

All statistics were two-tailed. Shapiro-Wilk test was used to test whether data followed a normal distribution and Levene's F test was used to test whether data met variance homogeneity. All statistical analyses were performed by using GraphPad Prism software (San Diego, California, USA).

Author affiliations

¹Metabolomics and Cell Biology Platforms, Gustave Roussy, Villejuif, France

²Centre de Recherche des Cordeliers, Equipe labellisée par la Ligue contre le cancer, Université Paris Cité, Sorbonne Université, Inserm U1138, Institut Universitaire de France, Paris, France

³Department of Respiratory and Critical Care Medicine, Union Hospital, Tongji Medical College, Huazhong University of Science and Technology, Wuhan, Hubei, China

⁴Faculté de Médecine, Université de Paris Saclay, Kremlin Bicêtre, France

⁵Cell death and Inflammation Unit, VIB-UGent Center for Inflammation Research, Ghent, Belgium

⁶Department of Biomedical Molecular Biology, Ghent University, Ghent, Belgium

⁷Surgical Oncology Department, Sir Run Run Shaw Hospital, Zhejiang University, Hangzhou, Zhejiang, China

⁸INSERM U1015, Equipe labellisée par la Ligue contre le cancer, Gustave Roussy, Villejuif, France

⁹ClinicObiome, Gustave-Roussy, Villejuif, France

¹⁰Institut du Cancer Paris CARPEM, Department of Biology, Hôpital Européen Georges Pompidou, AP-HP, Paris, France

Contributors SZ conducted experiments and analyses. LZ, MG and PL contributed to in vivo evaluations. SL conducted bioinformatic analysis. WX contributed to high throughput screening (HTS). A-LT, JP, HC, HP, MM and YL contributed to tissue preparation and sample analysis. YL conducted genotyping. LZ, YJ, OK and GK supervised the study and prepared the manuscript. GK and OK are the guarantors for this manuscript.

Funding SZ is supported by the Scientific Research Training Program for Young Talents of Wuhan Union Hospital. SJ, HC, HP, MM are supported by the China Scholarship Council. OK receives grants by the DIM ELICIT initiative of the Ile de France and Institut National du Cancer (INCa). GK is supported by the Ligue contre le Cancer (équipe labellisée); Agence Nationale de la Recherche (ANR) – Projets blancs; AMMICa US23/CNRS UMS3655; Association pour la recherche sur le cancer (ARC); Cancéropôle Ile-de-France; Fondation pour la Recherche Médicale (FRM); a donation by Elior; Equipex OncoPheno-Screen; European Joint Programme on Rare Diseases (EJPRD); European Research Council Advanced Investigator Award (ERC-2021-ADG, ICD-Cancer, Grant No. 101052444), European Union Horizon 2020 Projects Oncobiome, Prevalung (grant No. 101095604) and Crimson; Fondation Carrefour; Institut National du Cancer (INCa); Institut Universitaire de France; LabEx ImmunoOncology (ANR-18-IDEX-0001); a Cancer Research ASPIRE Award from the Mark Foundation; the RHU Immunolife; Seerave Foundation; SIRIC Stratified Oncology Cell DNA Repair and Tumor Immune Elimination (SOCRATE); and SIRIC Cancer Research and Personalized Medicine (CARPEM). This study contributes to the IdEx Université de Paris ANR-18-IDEX-0001.

Competing interests OK is a co-founder of Samsara Therapeutics. GK has been holding research contracts with Daiichi Sankyo, Eleor, Kaleido, Lytx Pharma, PharmaMar, Osasuna Therapeutics, Samsara Therapeutics, Sanofi, Tollys, and Vascage. GK has been consulting for Reithera. GK is on the Board of Directors of the Bristol Myers Squibb Foundation France. GK is a scientific co-founder of everImmune, Osasuna Therapeutics, Samsara Therapeutics and Therafast Bio. GK is the inventor of patents covering therapeutic targeting of aging, cancer, cystic fibrosis and metabolic disorders. GK's wife, Laurence Zitvogel, has held research contracts with 9 Meters Biopharma, Daiichi Sankyo, Pilege, was on the Board of Directors of Transgene, is a co-founder of everImmune, and holds patents covering the treatment of cancer and the therapeutic manipulation of the microbiota. GK's brother, Romano Kroemer, was an employee of Sanofi and now consults for Boehringer-Ingelheim.

Patient consent for publication Not applicable.

Ethics approval Not applicable.

Provenance and peer review Not commissioned; externally peer reviewed.

Data availability statement All data relevant to the study are included in the article or uploaded as supplementary information.

Supplemental material This content has been supplied by the author(s). It has not been vetted by BMJ Publishing Group Limited (BMJ) and may not have been peer-reviewed. Any opinions or recommendations discussed are solely those of the author(s) and are not endorsed by BMJ. BMJ disclaims all liability and responsibility arising from any reliance placed on the content. Where the content includes any translated material, BMJ does not warrant the accuracy and reliability of the translations (including but not limited to local regulations, clinical guidelines, terminology, drug names and drug dosages), and is not responsible for any error and/or omissions arising from translation and adaptation or otherwise.

Open access This is an open access article distributed in accordance with the Creative Commons Attribution Non Commercial (CC BY-NC 4.0) license, which permits others to distribute, remix, adapt, build upon this work non-commercially, and license their derivative works on different terms, provided the original work is properly cited, appropriate credit is given, any changes made indicated, and the use is non-commercial. See <http://creativecommons.org/licenses/by-nc/4.0/>.

ORCID iDs

Wei Xie <http://orcid.org/0000-0001-5554-2075>

Jonathan G Pol <http://orcid.org/0000-0002-8355-7562>

Hui Chen <http://orcid.org/0000-0002-1260-8617>

Yang Jin <http://orcid.org/0000-0003-2409-7073>

Oliver Kepp <http://orcid.org/0000-0002-6081-9558>

REFERENCES

- Casares N, Pequignot MO, Tesniere A, et al. Caspase-dependent Immunogenicity of doxorubicin-induced tumor cell death. *J Exp Med* 2005;202:1691–701.
- Obeid M, Tesniere A, Ghiringhelli F, et al. Calreticulin exposure dictates the Immunogenicity of cancer cell death. *Nat Med* 2007;13:54–61.
- Obeid M, Panaretakis T, Joza N, et al. Calreticulin exposure is required for the Immunogenicity of gamma-irradiation and UVC light-induced apoptosis. *Cell Death Differ* 2007;14:1848–50.
- Apetoh L, Ghiringhelli F, Tesniere A, et al. Toll-like receptor 4-dependent contribution of the immune system to anticancer chemotherapy and radiotherapy. *Nat Med* 2007;13:1050–9.
- Zitvogel L, Apetoh L, Ghiringhelli F, et al. The anticancer immune response: indispensable for therapeutic success *J Clin Invest* 2008;118:1991–2001.
- Galluzzi L, Humeau J, Buqué A, et al. Immunostimulation with chemotherapy in the era of immune Checkpoint inhibitors. *Nat Rev Clin Oncol* 2020;17:725–41.
- Galluzzi L, Vacchelli E, Bravo-San Pedro J-M, et al. Classification of current anticancer Immunotherapies. *Oncotarget* 2014;5:12472–508.
- Sharma P, Allison JP. Immune Checkpoint targeting in cancer therapy: toward combination strategies with curative potential. *Cell* 2015;161:205–14.
- Weber EW, Maus MV, Mackall CL. The emerging landscape of immune cell therapies. *Cell* 2020;181:46–62.
- Overwijk WW, Tagliaferri MA, Zalevsky J. Engineering IL-2 to give new life to T cell Immunotherapy. *Annu Rev Med* 2021;72:281–311.
- Korman AJ, Garrett-Thomson SC, Lonberg N. Author correction: the foundations of immune Checkpoint blockade and the Ipilimumab approval Decennial. *Nat Rev Drug Discov* 2022;21:163.
- Kroemer G, Galassi C, Zitvogel L, et al. Immunogenic cell stress and death. *Nat Immunol* 2022;23:487–500.
- Finck AV, Blanchard T, Roselle CP, et al. Engineered cellular Immunotherapies in cancer and beyond. *Nat Med* 2022;28:678–89.
- Kepp O, Zitvogel L, Kroemer G. Lurbinectedin: an FDA-approved inducer of Immunogenic cell death for the treatment of small-cell lung cancer. *Oncoimmunology* 2020;9:1795995.
- Offringa R, Kötznér L, Huck B, et al. The expanding role for small molecules in Immuno-oncology. *Nat Rev Drug Discov* 2022;21:821–40.
- Le Naour J, Liu P, Zhao L, et al. A Tir3 ligand Reestablishes chemotherapeutic responses in the context of Fpr1 deficiency. *Cancer Discov* 2021;11:408–23.
- Zhao L, Liu P, Xie W, et al. A genotype-phenotype screening system using conditionally immortalized immature Dendritic cells. *STAR Protoc* 2021;2:100732.
- Richter C, Thieme S, Bandola J, et al. Generation of inducible immortalized Dendritic cells with proper immune function in vitro and in vivo. *PLoS One* 2013;8:e62621.
- Karttunen J, Sanderson S, Shastri N. Detection of rare antigen-presenting cells by the lacZ T-cell activation assay suggests an expression cloning strategy for T-cell antigens. *Proc Natl Acad Sci U S A* 1992;89:6020–4.
- Wang C, Niederstrasser H, Douglas PM, et al. Small-molecule TFEB pathway agonists that ameliorate metabolic syndrome in mice and extend *C. Elegans* LifeSpan. *Nat Commun* 2017;8:2270.
- Jiang S-H, Dong F-Y, Da L-T, et al. Ikarugamycin inhibits Pancreatic cancer cell Glycolysis by targeting Hexokinase 2. *FASEB J* 2020;34:3943–55.
- Richards DM, Brogden RN, Heel RC, et al. A review of its pharmacodynamic properties and therapeutic efficacy. *Drugs* 1984;27:210–31.
- García-Ferreiro RE, Kerschensteiner D, Major F, et al. Mechanism of block of Heag1 K⁺ channels by Imipramine and Astemizole. *J Gen Physiol* 2004;124:301–17.
- Wang Z, Xu F, Hu J, et al. Modulation of lactate-Lysosome axis in Dendritic cells by Clotrimazole potentiates antitumor immunity. *J Immunother Cancer* 2021;9:e002155.
- Szabo SJ, Kim ST, Costa GL, et al. A novel transcription factor, T-bet, directs Th1 lineage commitment. *Cell* 2000;100:655–69.
- Lewis RS. Calcium signaling mechanisms in T lymphocytes. *Annu Rev Immunol* 2001;19:497–521.
- Jones AW. Perspectives in drug development and clinical pharmacology: the discovery of histamine H1 and H2 antagonists. *Clin Pharmacol Drug Dev* 2016;5:5–12.
- Li H, Xiao Y, Li Q, et al. The allergy mediator histamine confers resistance to Immunotherapy in cancer patients via activation of the macrophage histamine receptor H1. *Cancer Cell* 2022;40:36–52.

- 29 Verdoodt F, Dehlendorff C, Jäättelä M, *et al.* Antihistamines and ovarian cancer survival: nationwide cohort study and in vitro cell viability assay. *J Natl Cancer Inst* 2020;112:964–7.
- 30 Ellegaard A-M, Dehlendorff C, Vind AC, *et al.* Repurposing Cationic Amphiphilic Antihistamines for cancer treatment. *EBioMedicine* 2016;9:130–9.
- 31 Chiang C-H, Chiang C-H, Peng C-Y, *et al.* Efficacy of Cationic Amphiphilic Antihistamines on outcomes of patients treated with immune Checkpoint inhibitors. *Eur J Cancer* 2022;174:1–9.
- 32 Wan R, Wu J, Ouyang M, *et al.* Biophysical basis underlying dynamic Lck activation visualized by Zaplck FRET Biosensor. *Sci Adv* 2019;5:eaau2001.
- 33 Liu P, Zhao L, Senovilla L, *et al.* In vivo imaging of orthotopic lung cancer models in mice. *Methods Mol Biol* 2021;2279:199–212.
- 34 Son Y-I, Egawa S, Tatsumi T, *et al.* A novel bulk-culture method for generating mature Dendritic cells from Mouse bone marrow cells. *J Immunol Methods* 2002;262:145–57.
- 35 Lewis MD, de Leenheer E, Fishman S, *et al.* A reproducible method for the expansion of Mouse Cd8+ T lymphocytes. *J Immunol Methods* 2015;417:134–8.
- 36 Ghosh M, Shapiro LH. In vitro AG cross-presentation and in vivo AG cross-presentation by Dendritic cells in the Mouse. *BIO-PROTOCOL* 2012;2.
- 37 Humeau J, Sauvat A, Cerrato G, *et al.* Inhibition of transcription by Dactinomycin reveals a new characteristic of Immunogenic cell stress. *EMBO Mol Med* 2020;12:e11622.
- 38 Aran D, Hu Z, Butte AJ. xCell: Digitally portraying the tissue cellular heterogeneity landscape. *Genome Biol* 2017;18:220.
- 39 Li T, Fu J, Zeng Z, *et al.* Timer2.0 for analysis of tumor-infiltrating immune cells. *Nucleic Acids Res* 2020;48:W509–14.
- 40 Wherry EJ, Ha S-J, Kaech SM, *et al.* Molecular signature of Cd8+ T cell exhaustion during chronic viral infection. *Immunity* 2007;27:670–84.
- 41 Yu G, Wang LG, Han Y, *et al.* clusterProfiler: an R package for comparing biological themes among gene clusters. *OMICS* 2012;16:284–7.
- 42 Love MI, Huber W, Anders S. Moderated estimation of fold change and dispersion for RNA-Seq data with Deseq2. *Genome Biol* 2014;15:550.
- 43 Subramanian A, Tamayo P, Mootha VK, *et al.* Gene set enrichment analysis: a knowledge-based approach for interpreting genome-wide expression profiles. *Proc Natl Acad Sci U S A* 2005;102:15545–50.

Supplemental figure legends

Figure S1. Control experiments confirming the effects of ikarugamycin on dendritic cells. (A) De-iniDCs were treated with DMSO or ikarugamycin (IKA; 0.1, 0.2, 0.5, 1 μ M, from MedChemExpress, MCE, and Cayman) for 16 h, then washed twice and pulsed with OVA protein for 4 h, washed again twice, and then co-cultured with B3Z hybridoma cells. Interleukin-2 (IL2) secretion was measured by ELISA. (B) Gating strategy for the identification of bone marrow derived dendritic cell (BMDC) maturation (CD11c⁺CD40⁺, CD11c⁺CD80⁺, CD11c⁺CD86⁺, CD11c⁺MHC-II⁺) among viable BMDCs (Live/dead⁻). (C) The median MFI of CD40, CD80, CD86 and MHC-II of ikarugamycin (IKA; 1 μ M), astemizole (AST; 1 μ M) or lipopolysaccharide (LPS; 1 μ g/mL) treated BMDCs. (D) De-iniDCs were treated with DMSO or ikarugamycin (IKA; 1 μ M) for 16 h, then viability (Live/dead) was assessed using flow cytometry. (E) De-iniDCs were treated with polymyxin B (500 IU/mL) alone or in combination with IKA (0.5, 1 μ M) for 16 h, when cell supernatants were collected for the quantification of IL2. (F) Gating strategy for the identification of de-iniDC maturation (the median MFI of CD40, CD80, CD86, MHC-II) among viable de-iniDCs (CD11c⁺Live/dead⁻). (G-J) de-iniDCs were treated with polymyxin B (5 μ M) alone or in combination with IKA (0.5, 1 μ M) and lipopolysaccharide (LPS, 1 μ g/mL) for 16 h. Then the cells were analyzed for expression of the indicated proteins or cytokines using flow cytometry. (K-N) BMDCs were treated with polymyxin B (500 IU/mL) alone or in combination with IKA (0.5, 1 μ M) and lipopolysaccharide (LPS, 1 μ g/mL) for 16 h. Then the cells were analyzed for expression of the indicated proteins or cytokines using flow cytometry. (O) *B2m* gene knockout iniDCs or WT iniDCs were either or not treated with the stimulation of recombinant mouse IFN-gamma at a concentration of

1000 IU/mL for 20 h, and analyzed for expression of the beta-2 microglobulin protein using flow cytometry. **(P)** B2m knockout de-iniDCs (B2m^{-/-} de-iniDCs) were treated with DMSO or ikarugamycin (IKA; 0.1, 0.2, 0.5, 1 μ M, from MedChemExpress, ENZO and Cayman) for 16 h, then washed twice and pulsed with OVA or 10 ng/mL OVA257-264 peptide (SL8, as a positive control) for 4 h, washed again twice, and then co-cultured with B3Z hybridoma cells. IL2 secretion was measured by ELISA as an indication for antigen cross-presentation capacity. Data are reported as mean \pm SD, and statistical analyses were performed with two-tailed unpaired Student's t test (**A, C, P**), and one-way ANOVA followed by the Holm-Šídák post hoc test (**E, G-N**).

Figure S2. (A, B) The individual tumor growth curves of murine MCA205 fibrosarcoma treated with ikarugamycin alone or in combination with oxaliplatin. **(C)** Gating strategy for the identification of DC maturation (CD11c⁺CD86⁺) among F4/80 negative viable leukocytes (Live/dead⁻CD45⁺ F4/80⁻) in the tumor. **(D)** MCA205 fibrosarcoma bearing mice were treated as in **(A, B)** and were euthanized on day 15 after tumor injection, tumor was harvested and dissociated into single cell suspensions, and analyzed for expression of the indicated proteins using flow cytometry. **(E, F)** The individual tumor growth curves of murine MCA205 fibrosarcoma treated with ikarugamycin plus oxaliplatin alone or in combination with neutralizing antibodies to CD4 and CD8. Data are reported as the mean \pm SD, and statistical analyses were performed with one-way ANOVA followed by the Holm-Šídák post hoc test (**D**).

Figure S3. (A) Gating strategy for the identification of T cell activation (CD69⁺, interferon gamma (IFN γ)⁺) among viable primary CD8⁺ T cells (Live/dead⁻). **(B)** Mouse primary CD8⁺ T cells were labeled with 5 μ M 5-(and 6)-carboxyfluorescein diacetate succinimidyl ester of CFDA SE (CFSE), then cells were treated with DMSO, or AST (0.5, 1 μ M) or 1 μ g/mL anti-CD3 plus 0.5 μ g/mL anti-CD28 for 48 h, and analyzed for CFSE signal using flow cytometry. **(C)** Gating strategy for the identification of T cell activation (CD69⁺, ICOS⁺, TBX21⁺, IFN γ)⁺) among viable CD4⁺ or CD8⁺ T cells (Live/dead⁻CD3⁺ CD4⁺CD8⁻ or Live/dead⁻CD3⁺ CD4⁻CD8⁺).

Figure S4. (A) Gating strategy for the identification of LCK activation (CFP/FRET) among Jurkat-LCK T cells. **(B)** Gating strategy for the identification of T cell activation (CD69⁺, IFN γ)⁺) among viable B3Z hybridoma T cells (Live/dead⁻). **(C)** Jurkat T cells stained with Indo-1 AM (1 μ M) calcium indicator were treated with astemizole (AST, 1 μ M) or ionomycin (Iono, 100 nM) and analyzed by flow cytometry. **(D, E)** B3Z hybridoma cells were treated with astemizole (1 μ M) alone or in combination with BAPTA-AM (0.5, 1, 2, 5 μ M) for 16 h, the cell supernatants were collected for the quantification of IL2 secretion by ELISA **(D)**. While the remaining cells were treated with brefeldin A (5 μ g/mL) for 5 h, and analyzed for expression of IFN γ using flow cytometry **(E)**. Data are reported as the mean \pm SD, and statistical analyses were performed with one-way ANOVA followed by the Holm-Šidák post hoc test.

Figure S5. Astemizole activate T cell via HRH1 receptor. (A, B) B3Z hybridoma cells were treated with astemizole (1 μ M) alone or in combination with 2-pyridylethylamine dihydrochloride (0.05, 0.1, 0.2, 0.5, 1 mM) for 16 h, the cell supernatants were collected

for the quantification of IL2 secretion by ELISA **(A)**. While the remaining cells were treated with brefeldin A (5 $\mu\text{g}/\text{mL}$) for 5 h, and analyzed for expression of IFN γ using flow cytometry **(B)**. **(C-F)** B3Z hybridoma cells were treated with astemizole (1 μM) alone or in combination with Amthamine dihydrobromide **(C)**, Dimaprit dihydrochloride **(D)**, Imetit dihydrobromide **(E)** or 4-methylhistamine **(F)** (1, 2, 5, 10 μM) for 16 h, the cell supernatants were collected for the quantification of IL2 secretion by ELISA. **(G)** PCR analysis of genomic DNA from wild-type and *hrh1* knockout mice. **(H)** Gating strategy for the identification of IFN γ^+ expression among viable CD4 $^+$ or CD8 $^+$ T cells (Live/dead $^-$ CD3 $^+$ CD4 $^+$ CD8 $^-$ or Live/dead $^-$ CD3 $^+$ CD4 $^+$ CD8 $^+$) and the FOXP3 expression among viable CD4 $^+$ T cells. Data are reported as the mean \pm SD, and statistical analyses were performed with one-way ANOVA followed by the Holm-Šidák post hoc test.

Figure S6. Astemizole enhances anti-tumor effect of immunogenic chemotherapy. **(A, B)** The individual tumor growth curves of murine MCA205 fibrosarcoma treated with astemizole alone or in combination with oxaliplatin. **(C)** Gating strategy for the identification of T cell activation (CD69 $^+$ CD8 $^+$, ICOS $^+$ CD8 $^+$, IFN γ^+ CD8 $^+$) as well as Tregs (FOXP3 $^+$ CD4 $^+$) among viable leukocytes (Live/dead $^-$ CD45 $^+$) in the tumor. **(D)** Gating strategy for the identification of DC maturation (CD11c $^+$ MHC-II $^+$) among F4/80 negative viable leukocytes (Live/dead $^-$ CD45 $^+$ F4/80 $^-$) and Tregs (FOXP3 $^+$ CD4 $^+$) among viable leukocytes (Live/dead $^-$ CD45 $^+$) in the tumor draining lymph node. **(E, F)** MCA205 fibrosarcoma bearing mice were treated as in **(Figure 6A)** and were euthanized on day 15 after tumor injection, tumor draining lymph node were harvested and dissociated into single cell suspensions, and analyzed for expression of the indicated proteins or cytokines

using flow cytometry. **(G)** Schematic overview of the treatment of murine TC-1 lung cancer with astemizole and oxaliplatin, anti-PD-1, alone or in combination. The individual tumor growth curves **(H-J)**, the tumor growth curves **(K, mean \pm SEM)** and Kaplan-Meier overall survival **(L)** of murine TC-1 lung cancer in C57BL/6 mice. **(M)** Schematic overview of the treatment of murine E0771 breast cancer with astemizole and oxaliplatin, alone or in combination. **(N-Q)** The individual tumor growth curves **(N, O)**, the tumor growth curves **(P, mean \pm SEM)** and Kaplan-Meier overall survival **(Q)** of murine E0771 breast cancer in C57BL/6 mice. Data are reported as the mean \pm SD, and statistical analyses were performed with one-way ANOVA followed by the Holm-Šidák post hoc test **(E, F)**, and two-way ANOVA followed by the Holm-Šidák post hoc test **(K, P)**. Log-rank test was used for survival comparison **(L, Q)**.

Figure S7. Astemizole induces immune-dependent anticancer efficacy in orthotopic TC-1-luc lung cancer model. **(A, B)** The individual tumor growth curves of murine orthotopic TC-1-luc lung cancer treated with astemizole alone or in combination with oxaliplatin. **(C-I)** The individual tumor growth curves **(C-H)** and representative bioluminescence images **(I)** of murine orthotopic TC-1-luc lung cancer treated with astemizole plus oxaliplatin, in combination with neutralizing antibodies to CD4 and/or CD8, or the isotype control antibodies. **(J-L)** The individual tumor growth curves **(J, K)** and representative bioluminescence images **(L)** of murine orthotopic TC-1-luc lung cancer treated with astemizole plus oxaliplatin, in combination with neutralizing antibodies to IFN γ , or the isotype control antibodies.

Figure S8. Correlation of HRH1 expression with immune-related parameters in different cancer types. (A) Relationship between HRH1 and the abundance of distinct cancer types. Correlations of HRH1 mRNA expression and myeloid cells including dendritic cells (DCs) and macrophages as well as T cell subsets were calculated for distinct cancer types listed in TCGA. (B) Association of HRH1 expression and Tex-related genes. The heatmaps in A and B indicate the Spearman correlation coefficients (r) ranging from -1 to 1. (C) HRH1 mRNA levels predict T cell exhaustion across various cancer types. Patients were stratified into HRH1 high and HRH1 low groups for each cancer types. Enrichment of exhausted CD8 T cell signature: genes upregulated in exhausted vs effector CD8 T cells among HRH1 high vs low patients with different cancers is shown in bubble plot. The color scale represents p values, the point size represents gene counts for each signature.

Supplemental table 1. De-ini-dendritic cells (DC) were cultured with the compounds of the indicated chemical libraries for 16 h, then washed twice and pulsed with 500 $\mu\text{g/mL}$ ovalbumin (OVA) protein for 4 h, washed again twice, and then co-cultured with B3Z hybridoma cells for 16 h. Then, the supernatant of cells was harvested and the production of interleukin 2 (IL2), as an indicator for antigen cross-presentation capacity, was measured by enzyme-linked immunosorbent assay (ELISA). IL2 concentration was normalized according to dimethyl sulfoxide (DMSO)-treated controls. Data are reported as the mean of three replicates.

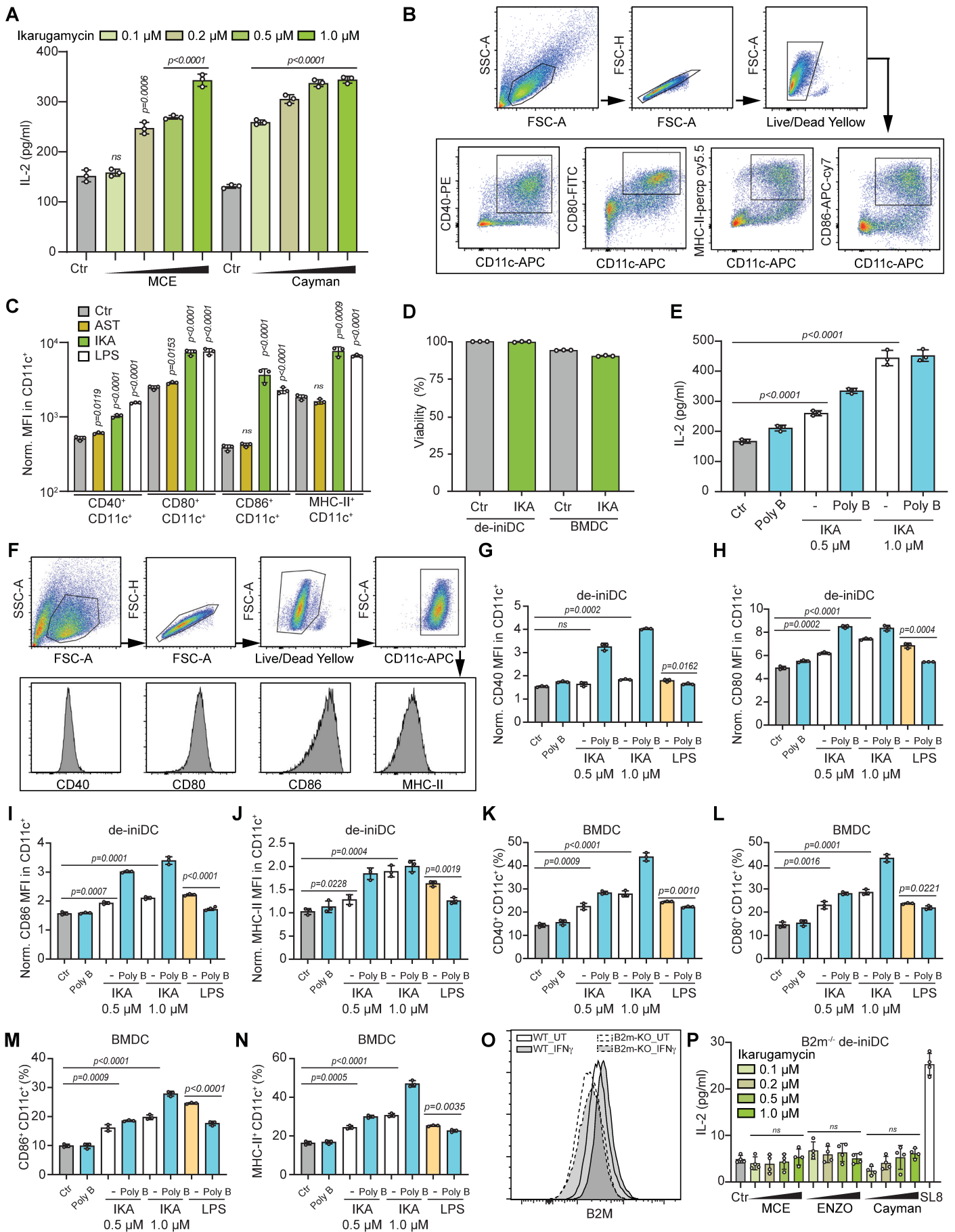


Figure S1

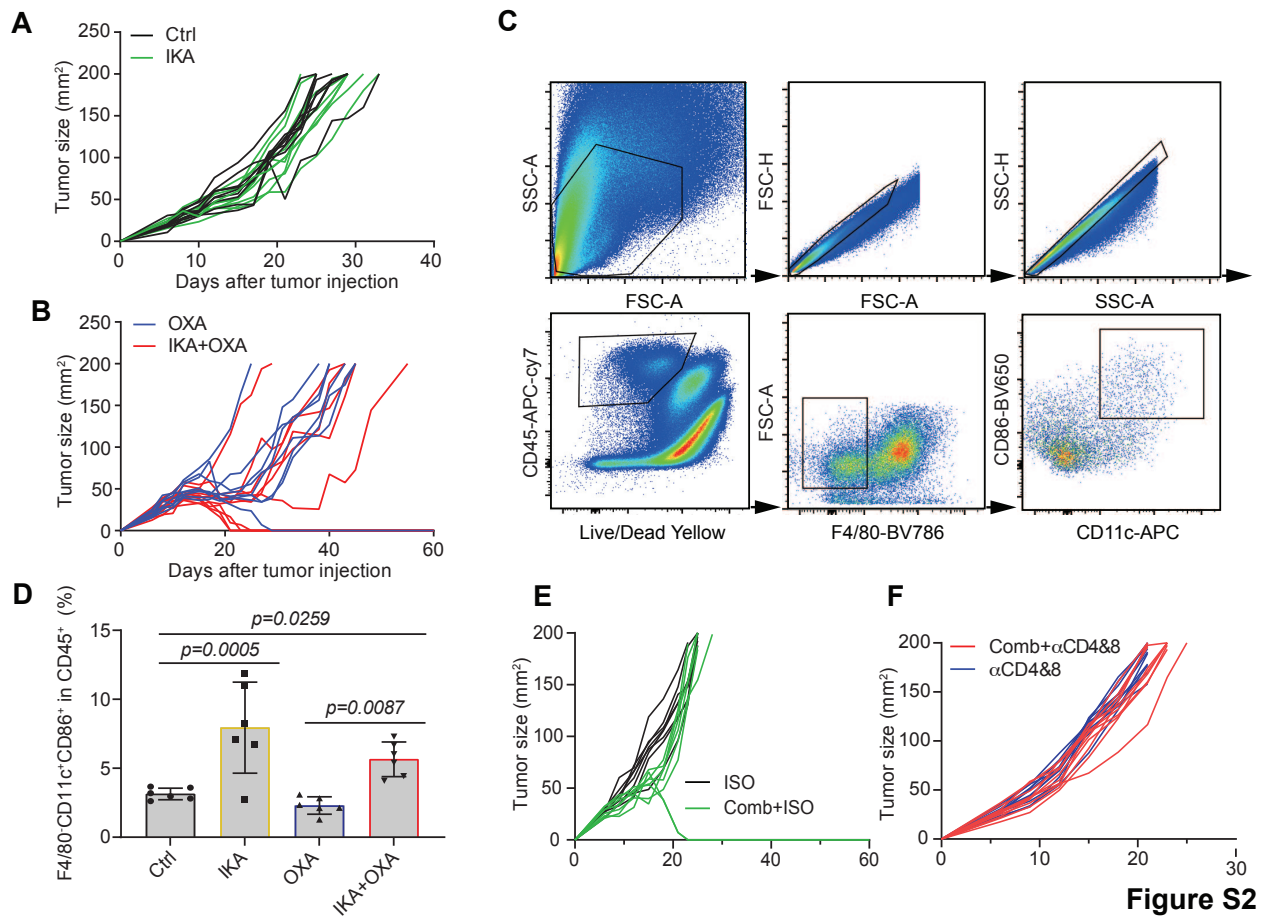


Figure S2

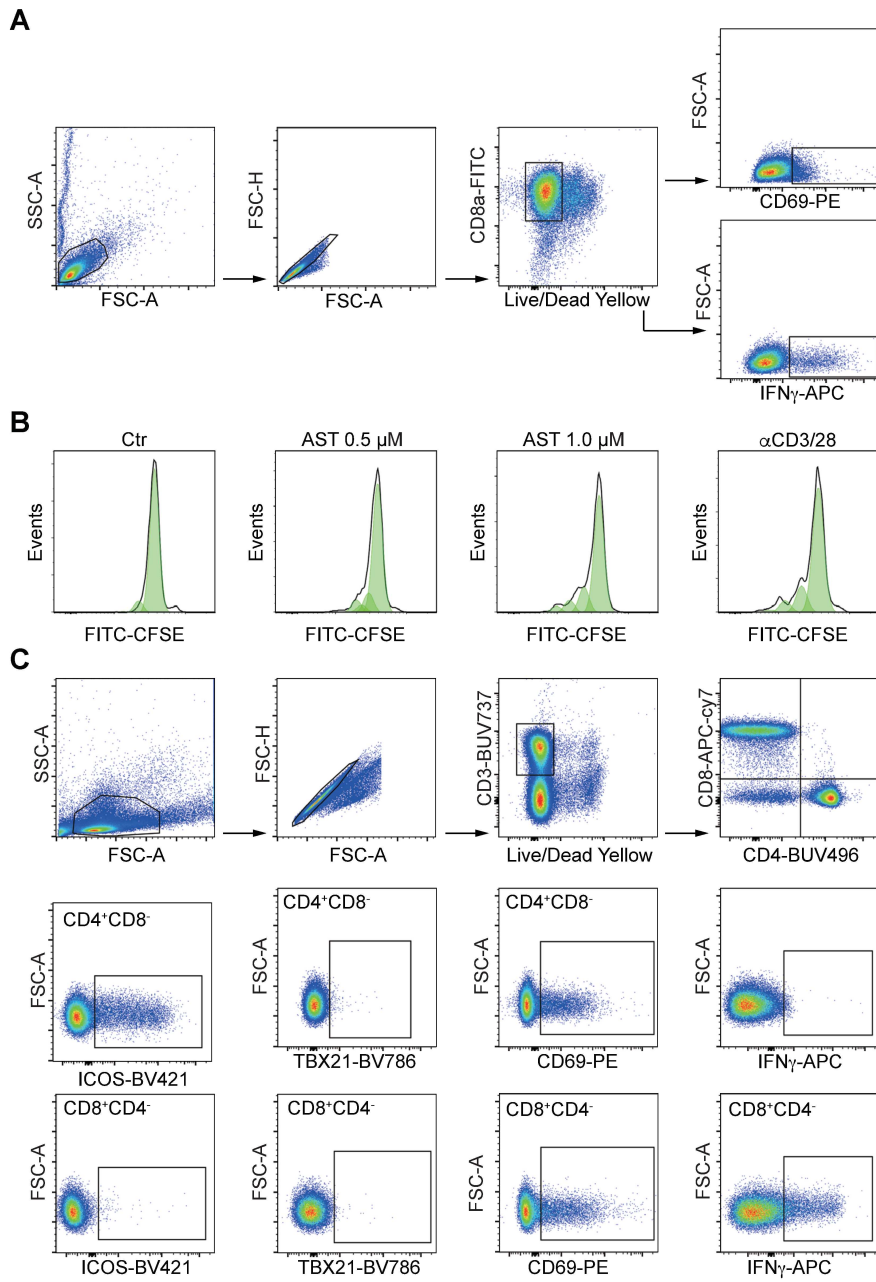


Figure S3

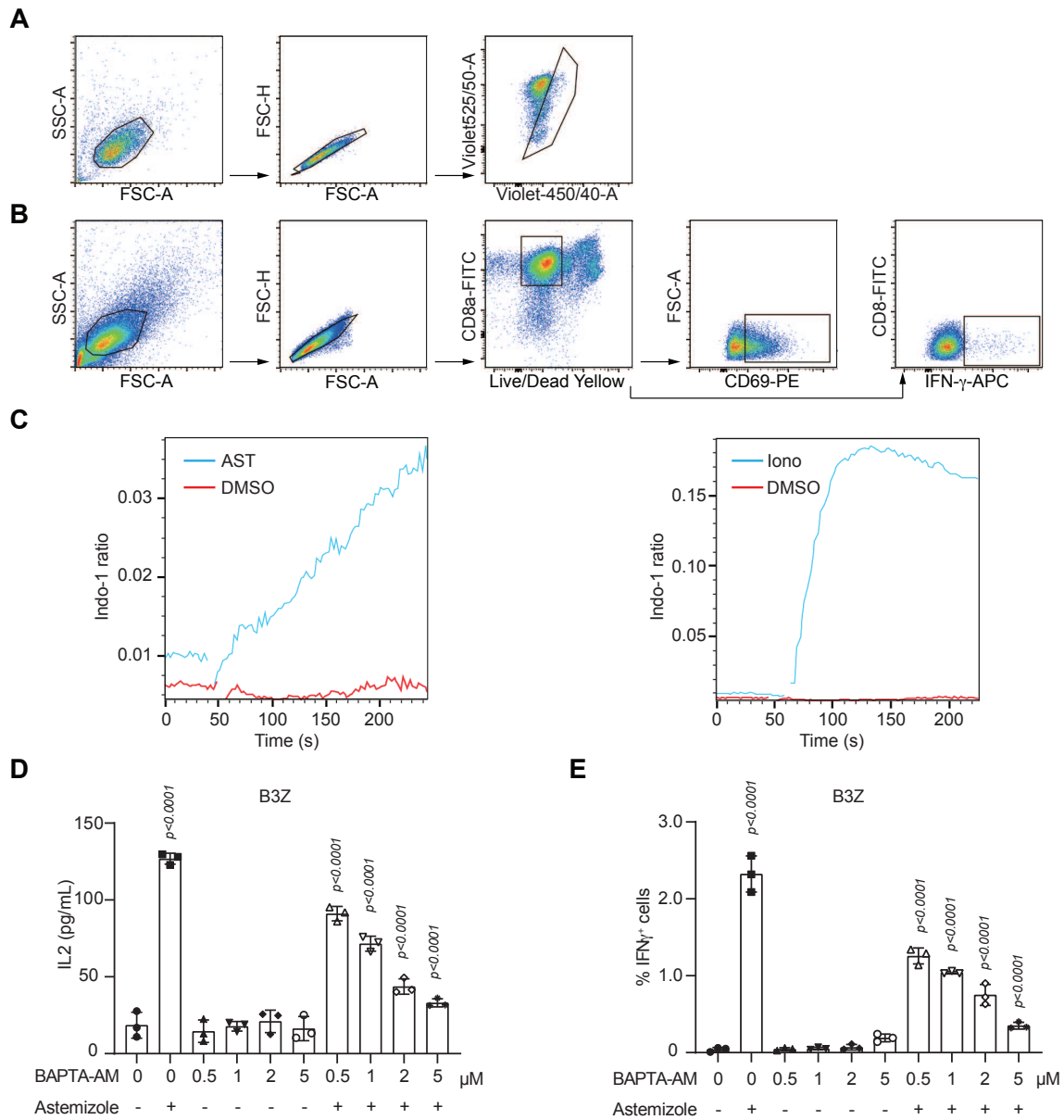


Figure S4

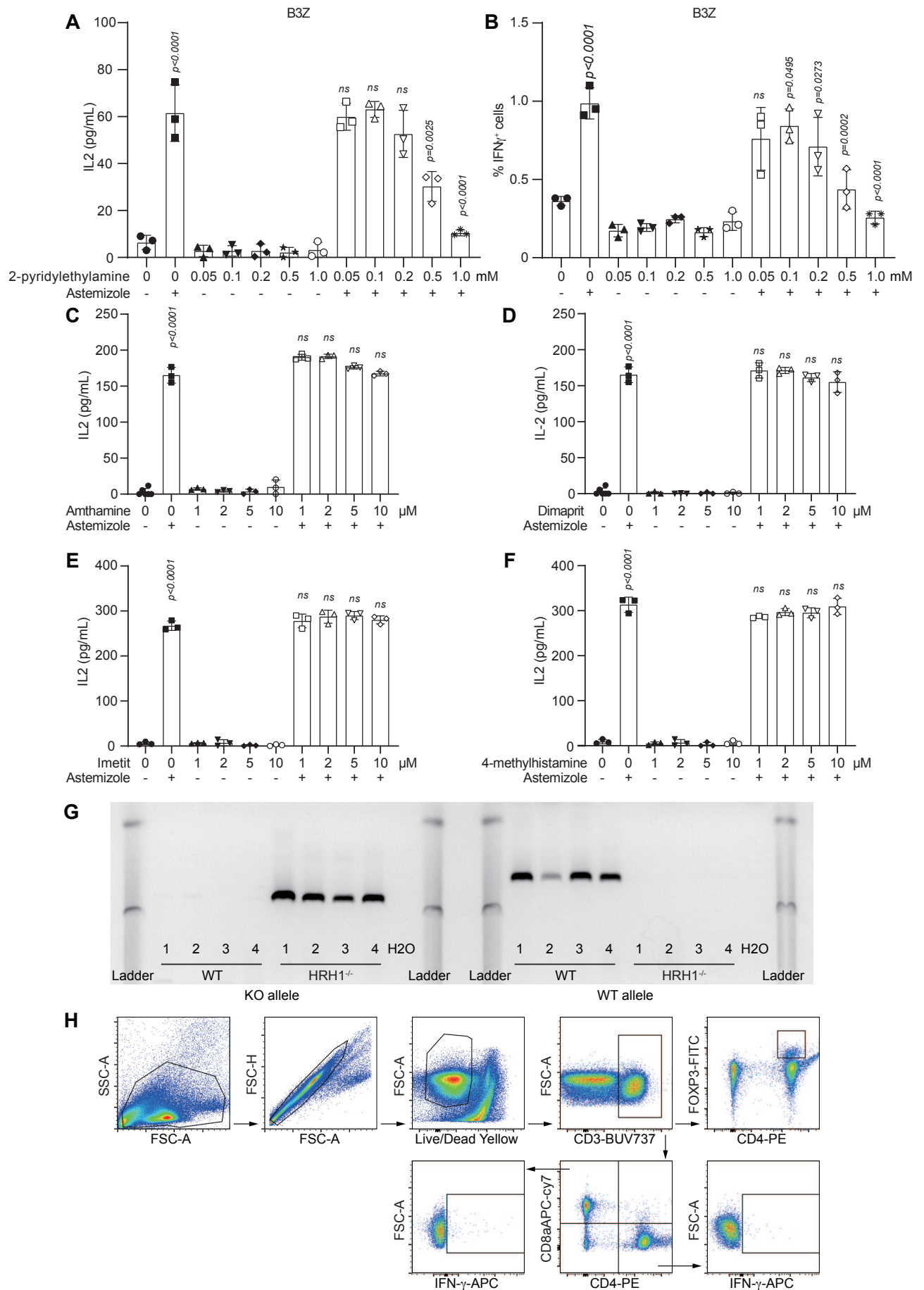


Figure S5

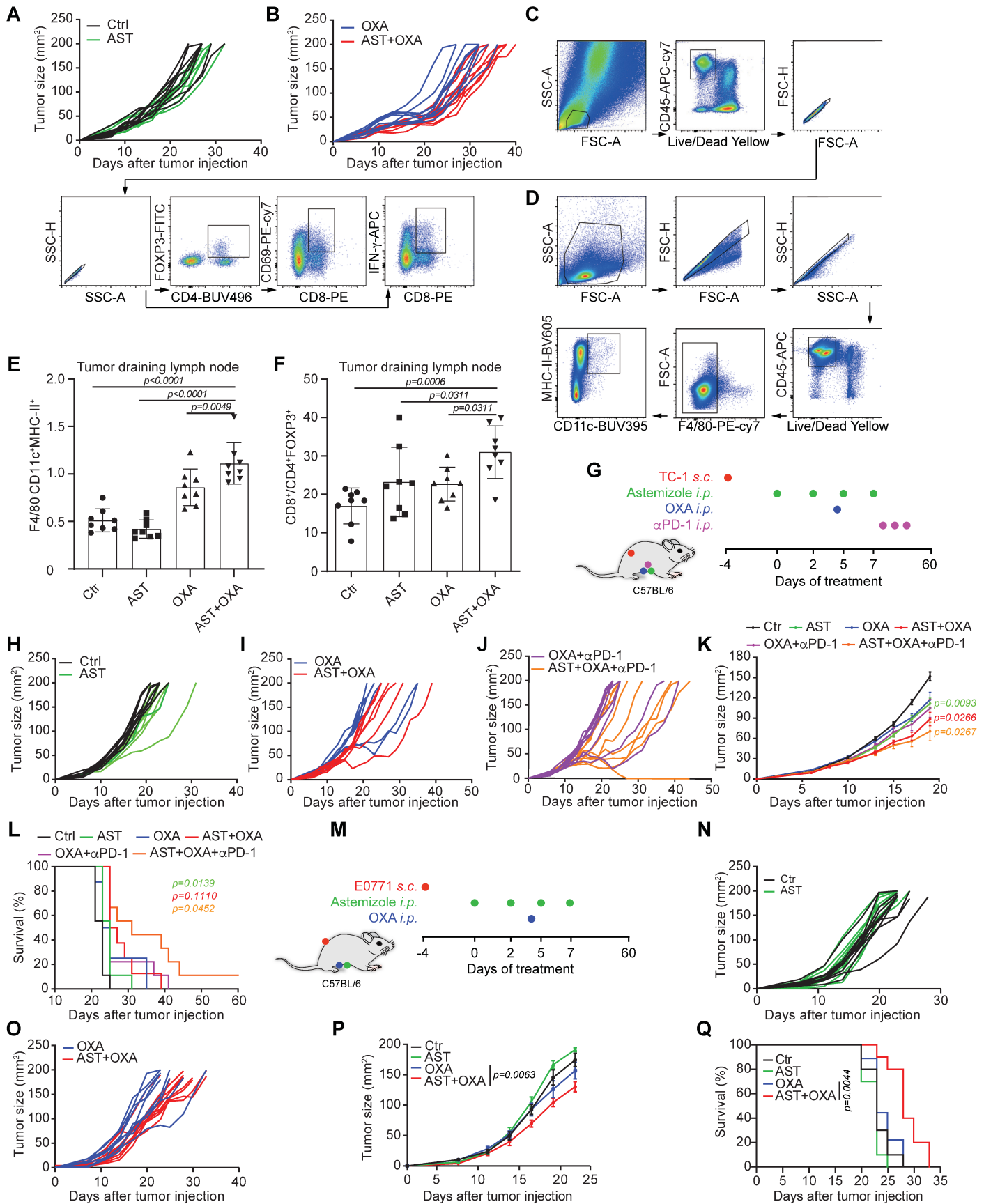


Figure S6

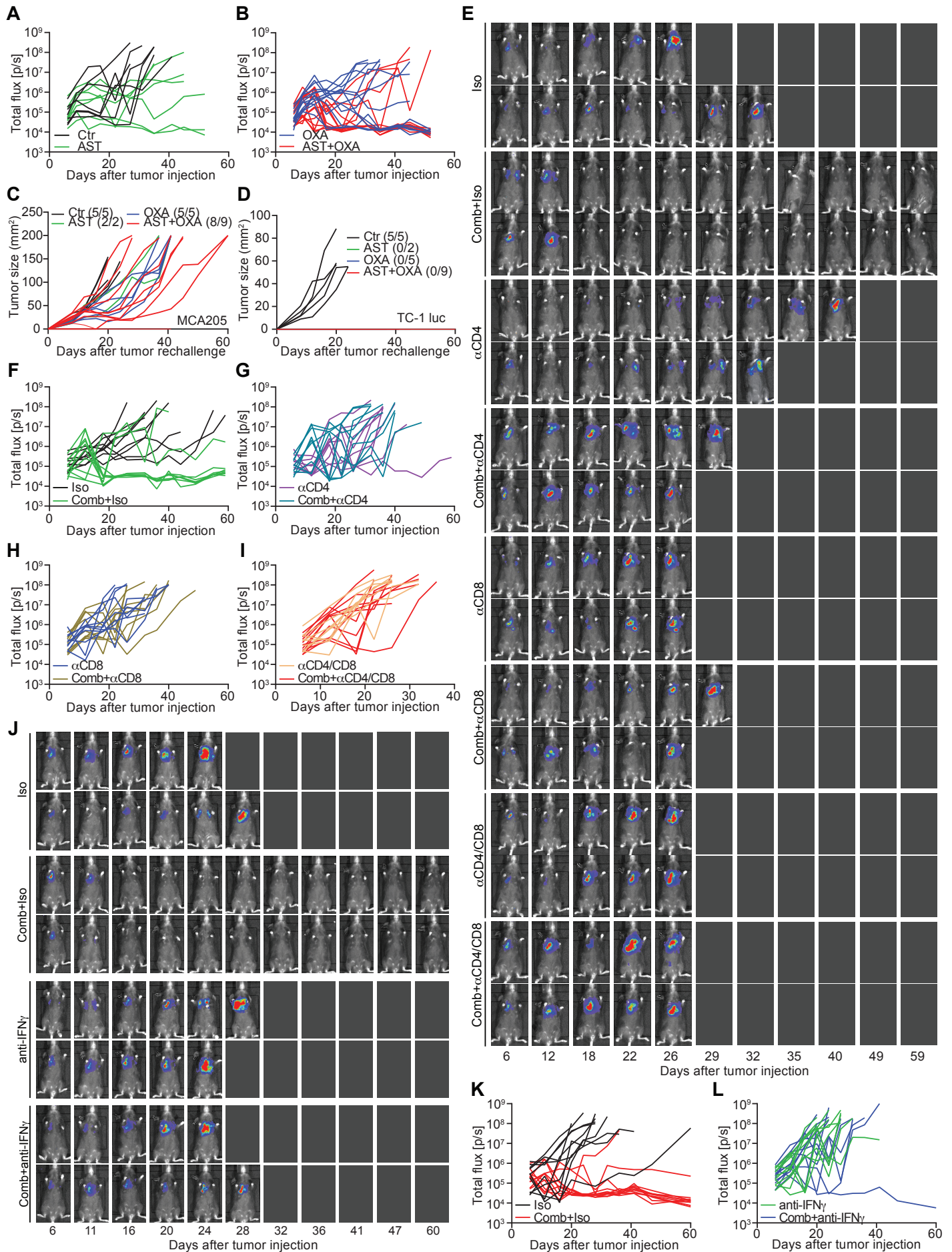


Figure S7

